The Astrophysical Journal, 681:1484–1504, 2008 July 10

SPITZER MIPS OBSERVATIONS OF STARS IN THE β PICTORIS MOVING GROUP

L. M. Rebull,[1] K. R. Stapelfeldt,[2] M. W. Werner,[2] V. G. Mannings,[1] C. Chen,[3]
J. R. Stauffer,[1] P. S. Smith,[4] I. Song,[1] D. Hines,[5] and F. J. Low[4]
Received 2007 July 18; accepted 2008 March 6

ABSTRACT

We present Multiband Imaging Photometer for *Spitzer* (MIPS) observations at 24 and 70 μm for 30 stars, and at 160 μm for a subset of 12 stars, in the nearby ($\sim$30 pc), young ($\sim$12 Myr) β Pictoris moving group (BPMG). In several cases, the new MIPS measurements resolve source confusion and background contamination issues in the *IRAS* data for this sample. We find that 7 members have 24 μm excesses, implying a debris disk fraction of 23%, and that at least 11 have 70 μm excesses (disk fraction of $\geq$37%). Five disks are detected at 160 μm (out of a biased sample of 12 stars observed), with a range of 160/70 flux ratios. The disk fraction at 24 and 70 μm, and the size of the excesses measured at each wavelength, are both consistent with an "inside-out" infrared excess decrease with time, wherein the shorter wavelength excesses disappear before longer wavelength excesses, and consistent with the overall decrease of infrared excess frequency with stellar age, as seen in *Spitzer* studies of other young stellar groups. Assuming that the infrared excesses are entirely due to circumstellar disks, we characterize the disk properties using simple models and fractional infrared luminosities. Optically thick disks, seen in the younger TW Hya and η Cha associations, are entirely absent in the BPMG. Additional flux density measurements at 24 and 70 μm are reported for nine Tucana-Horologium association member stars. Since this is <20% of the association membership, limited analysis on the complete disk fraction of this association is possible.

Subject headings: circumstellar matter — stars: individual (β Pictoris moving group)

1. INTRODUCTION

In recent years, several nearby ($\lesssim$100 pc) young ($\lesssim$200 Myr) stellar associations have been identified. These groupings provide a special opportunity to study "up close" the evolution of circumstellar material at a potentially crucial phase of disk evolution, namely, that epoch when planets are thought to be forming. With the advent of the *Spitzer Space Telescope* (Werner et al. 2004), specifically the Multiband Imaging Photometer for *Spitzer* (MIPS; Rieke et al. 2004), astronomers now can easily study the properties of the stars in those nearby groupings at much lower disk excess levels than was possible with the Two Micron All Sky Survey (2MASS) or the *Infrared Space Observatory* (*ISO*). In some cases, these stars are close enough, and the disks big enough, that one can spatially resolve the disk structure, providing even more information about the disk properties. While it is thought that all stars start with massive, optically thick, primordial disks, older stars possess much less massive, optically thin, second-generation, debris disks, in which the dust to primary star luminosity ratio $L_{\rm dust}/L_* \lesssim 10^{-3}$ (see, e.g., Meyer et al. 2007 and references therein). In this phase, it is thought that planetesimal-mass bodies have already formed in the disk; collisions of these bodies can replenish the dust in those systems. The evolution of mid- to far-infrared–emitting dust grains a few microns in size within debris disks has been a subject of much study (see, e.g., Bryden et al. 2006; Su et al. 2006; Chen et al. 2005a, 2005b; Werner et al. 2006 and references therein). The measurement of the overall disk fraction in clusters of known age (and ultimately measurement of the dust distribution in individual systems via direct imaging) is key to understanding disk evolution and planet formation.

The disk around β Pictoris has been known since the mid-1980s when it was one of the first debris disks discovered by the *Infrared Astronomy Satellite* (*IRAS*) mission (Gillett 1986; Paresce & Burrows 1987). Little was known about β Pic when its infrared excess was discovered. It was not located within an obvious star-forming region or cluster, and even its age was poorly constrained. New observations in recent years have placed β Pic in better context. A number of other stars have been discovered that share β Pic's space motion and are believed to be coeval with β Pic (e.g., Barrado y Navascues et al. 1999; Zuckerman et al. 2001b, and references therein). At only $\sim$30 pc away with an age of $\sim$12 Myr, this so-called β Pic moving group (BPMG) is the nearest identified young stellar association and has been studied intensively. Zuckerman & Song (2004) and subsequent authors have identified 30 BPMG member or potential member stellar systems.

This study presents MIPS observations at 24, 70, and 160 μm of all of the currently known BPMG members, as well as several members from the Tucana-Horologium association, another nearby ($\sim$50 pc) young ($\sim$30 Myr) group (Zuckerman & Song 2004). We first present the observational details (§ 2) and then discuss identification of stars with infrared excesses (§ 3). We fit some simple models in § 4 to characterize the disk properties for the stars we have found with excesses. Finally, we discuss the sample as a whole in § 5 and summarize our conclusions in § 6.

2. OBSERVATIONS, DATA REDUCTION, AND ANCILLARY DATA

2.1. *Target Selection and Observations*

Many individual member stars from nearby young stellar clusters are scattered among several of the programs originating with

[1] Spitzer Science Center, Mail Stop 220-6, California Institute of Technology, 1200 East California Boulevard, Pasadena, CA 91125; luisa.rebull@jpl.nasa.gov.
[2] Jet Propulsion Laboratory, California Institute of Technology, Pasadena, CA 91109.
[3] National Optical Astronomy Observatory, P.O. Box 26732, Tucson, AZ 85726-6732.
[4] Steward Observatory, University of Arizona, 933 North Cherry Avenue, Tucson, AZ 85721.
[5] Space Science Institute.

TABLE 1
NEARBY YOUNG ASSOCIATION MEMBERS IN THIS STUDY

Association	HIP Number	HD Number	HR Number	GJ Number	Other Name	Name Used Here	Distance (pc)	Spectral Type	V (mag)	K_s (mag)
BPMG	560	203	9			HR 9	39.1	F2 IV	6.2	5.24
BPMG	10679	[a]				HIP 10679	34.0	G2 V	7.8	6.26
BPMG	10680	14082				HD 14082	39.4	F5 V	7.0	5.79
BPMG	11437				AG Tri A	AG Tri A	42.3	K8	10.1	7.08
BPMG	11437				AG Tri B	AG Tri B	42.3	M0	...	7.92
BPMG	12545				BD 05 378	HIP 12545	40.5	M0	10.4	7.07
BPMG	21547	29391	1474		51 Eri	51 Eri	29.8	F0 V	5.2	4.54
BPMG				3305		GJ 3305	29.8	M0.5	10.6	6.41
BPMG	23309				CD −57 1054	HIP 23309	26.3	K8	10.1	6.24
BPMG	23418			3322		GJ 3322 A/B	32.1	M3 V	11.7	6.37
BPMG	25486	35850	1817			HR 1817	26.8	F7/8 V	6.3	4.93
BPMG	27321	39060			β Pic	β Pic	19.3	A5 V	3.9	3.53
BPMG	29964	45081			AO Men	AO Men	38.5	K7	9.9	6.81
BPMG	76629	139084			V343 Nor A	V343 Nor A/B	39.8	K0 V	8.2	5.85
BPMG	79881	146624	6070			HR 6070	43.1	A0 (V)	4.8	4.74
BPMG	84586	155555			V824 Ara A/B	V824 Ara A/B	31.4	K1 VP	6.9	4.70
BPMG	84586	155555			V824 Ara C	V824 Ara C	31.4	M4.5	12.7	7.63
BPMG	88399	164249				HD 164249	46.9	F5 V	7.0	5.91
BPMG	88726A	165189	6749			HR 6749/HR 6750	43.9	A5 V	5.0	4.39
BPMG	92024	172555	7012			HR 7012	29.2	A5 IV/V	4.8	4.30
BPMG					CD −64 1208AB	CD −64 1208 A/B	29.2	K7	10.4	6.10
BPMG	92680	174429			PZ Tel	PZ Tel	49.7	K0 VP	8.4	6.37
BPMG	95261	181296	7329		η Tel	η Tel A/B	47.7	A0 V	5.1	5.01
BPMG	95270	181327				HD 181327	50.6	F5/6 V	7.0	5.91
BPMG	102141	196982		799	AT Mic	AT Mic A/B	10.2	M4.5	10.3	4.94
BPMG	102409	197481		803	AU Mic	AU Mic	9.9	M1 Ve	8.8	4.53
BPMG	103311	199143				HD 199143 A/B	47.7	F8 V	7.3	5.81
BPMG		358623			AZ Cap A, BD 17 6128	AZ Cap A/B	47.7	K7/M0	10.6	7.04
BPMG	112312				WW PsA A	WW PsA A	23.6	M4e	12.2	6.93
BPMG	112312				WW PsA B	WW PsA B	23.6	M4.5e	13.4	7.79
Tuc-Hor	1113	987				HD 987	43.7	G6 V	8.7	6.96
Tuc-Hor	3556					HIP 3556	38.5	M3	12.3	7.62
Tuc-Hor					CPD −64 120	CPD −64 120	29.2	K7	9.5	8.01
Tuc-Hor	7805	10472				HD 10472	66.6	F2 IV/V	7.6	6.63
Tuc-Hor	9685	12894				HD 12894	47.2	F2 V	6.4	5.45
Tuc-Hor	10602	14228	674		ϕ Eri	Phi Eri	47.5	B8 V	3.6	4.13
Tuc-Hor					GSC 8056-0482	GSC 8056-0482	30.9	M3 Ve	12.1	7.50
Tuc-Hor	12394	16978	806		ϵ Hya	ϵ Hya	47.0	B9 V	4.1	4.25
Tuc-Hor	101612	195627	7848			HR 7848	27.6	F0 V	4.8	4.04

[a] Some references list this object as HD 14082B.

the *Spitzer* Guaranteed Time Observation (GTO) program. The *Spitzer* GTO program 102 (PI: M. Werner) observed 13 BPMG stars or systems, along with 9 stars (or systems) thought to be Tuc-Hor association members (where membership for both associations is as reported by Zuckerman & Song 2004). As the observers of record for this program, we felt it important to report the observations for all of the stars from included in it. In order to enhance the discussion, we assembled a list of all of the stars or stellar systems thought to be members of the BPMG, based on Zuckerman & Song (2004). We retrieved data for the remaining stars/star systems of the BPMG out of the *Spitzer* archive. Nearly all of these observations come from GTO programs and were obtained over the first 3 years of the mission.

The 39 stars or systems discussed in this paper—all the targets from program 102, plus the remaining β Pic member stars from the archive—are listed in Table 1, along with cluster membership. Note that binary systems unresolved by MIPS are listed together, e.g., GJ 3322 A/B, and that these unresolved binaries are effectively treated as single stars throughout the rest of this paper. The implications of this decision are discussed below. The Tuc-Hor stars are included at the bottom of this table (and the next two tables), separated from the BPMG stars by a line.

All of the Spitzer archive identifications (AORKEYs) and other assorted program information (including program identifications and dates of observation) are listed in Table 2. Since the observations were acquired from a variety of programs, the integration times used for each target are not uniform (see Table 2). All targets were observed at 24 μm, all but one at 70 μm (CPD −64 120), and a subset of 12, not selected uniformly, were observed at 160 μm. All objects are detected at good signal-to-noise ratio (S/N $>$ 25) at 24 μm; there are many upper limits at both 70 and 160 μm.

Since we assembled our list of members from Zuckerman & Song (2004), we are obviously missing any undiscovered members. Thus, we cannot maintain that our study is complete over all possible BPMG members. As discussed in I. Song et al. (2008, in preparation) and Torres et al. (2006), surveys of young stars near Earth form distinctive groupings in age-velocity-position space, and young members earlier than M are easily identified via, e.g., lithium absorption. It is unlikely that there are many undiscovered members earlier than M. However, it is possible that

TABLE 2
SUMMARY OF OBSERVATIONS

SPITZER PROGRAM ID	PI	AORKEY (*Spitzer* Archive Identifier)	DATE OF OBSERVATION	OBJECT(S)	INTEGRATION TIME (s)		
					24 μm	70 μm	160 μm
102	Werner	9018624, 9020928	2005 Dec 1, 2004 Jun 21	HR 9	48	126	63
3600	Song	11256064	2005 Jan 29	HD 14082, HIP 10679	48	231	0
102	Werner	9019392, 9020672	2005 Aug 29, 2006 Feb 18	AG Tri A/B	48	231	63
102	Werner	9017600, 9020160	2005 Sep 5, 2006 Feb 17	HIP 12545	48	231	63
102	Werner	9019904	2004 Sep 16	51 Eri, GJ 3305	48	231	0
102	Werner	9024000	2004 Nov 8	HIP 23309	48	126	0
102	Werner	9023744	2004 Oct 14	GJ 3322 A/B	48	126	0
148	FEPS	5252352, 5446656, 5447424	2005 Feb 27 (all three)	HR 1817	276	693	84
80	Werner	8970240, 12613632, 4884992	2004 Mar 20, 2005 Apr 4, 2004 Feb 21	β Pic	36	252	27
148	FEPS	5222656	2004 Oct 13	AO Men	92	881	84
148	FEPS	5223424	2004 Jul 29	V343 Nor A/B	92	231	0
10	Jura	3720704	2004 Feb 25	HR 6070	48	126	0
84	Jura	4813056	2004 Sep 17	V824 Ara A/B/C	48	126	0
102	Werner	9019136, 9023488	2005 Aug 30, 2004 Mar 17	HD 164249	48	101	63
102	Werner	9023232	2004 Sep 23	HR 6749/HR 6750	48	231	0
10	Jura	3723776	2004 Apr 7	HR 7012, CD -64 1208A/B	48	126	0
72	Low	4554496	2004 Apr 6	PZ Tel	180	545	0
57	Rieke	8934912, 8935168, 8935424	2004 Apr 9, Apr 9, Apr 7	η Tel	48	100	76
72	Low	4556032	2004 Apr 6	HD 181327	92	126	63
80	Werner	4637184	2004 May 11	AT Mic A/B	48	231	0
3657	Graham	11403008	2005 May 20	AU Mic (160 only)	0	0	629
80	Werner	4637440	2004 May 2	AU Mic	48	231	0
148	FEPS	5254656	2004 Oct 13	HD 199143 A/B	92	231	84
80	Werner	4643840	2004 May 11	AZ Cap A/B	48	545	0
102	Werner	9021696	2004 May 31	WW PsA A/B	48	126	0
102	Werner	9022976	2004 Nov 5	HD 987	48	126	0
102	Werner	9022720	2004 Nov 3	HIP 3556	48	231	0
102	Werner	9022464	2004 May 11	CPD -64 120	48	0	0
102	Werner	4945152	2004 Nov 7	HD 10472	48	69	0
102	Werner	9022208	2004 Nov 7	HD 12894	48	126	0
102	Werner	9021952	2004 Nov 8	ϕ Eri	48	231	0
102	Werner	9021440	2004 Nov 7	GSC 8056-482	48	126	0
102	Werner	9021184	2005 Jun 19	ϵ Hya	48	231	0
102	Werner	9020416	2004 Apr 13	HR 7848	48	69	0

there are undiscovered M star members. These intrinsically fainter M stars often lack parallax measurements and, moreover, are often harder to confirm as members, because they, for example, deplete Li faster than higher mass stars.

Because the BPMG is physically close to us, it subtends a large angle on the sky, and finding additional members often requires searching over a large area. However, comoving companions may be found in close proximity to known members, as evidenced by the number of known companions in the BPMG. Our observations cover relatively small regions around each member star, so we have a chance of finding these sorts of close companions. Several observations detect additional objects in the field near BPMG members; since these objects are bright enough to be detected in these shallow observations, these objects could also be potential association members, and the argument for BPMG membership might be made if these objects have infrared excesses. We examined our data for any additional stars with excesses serendipitously included in the *Spitzer* field of view, but none were detected; see the Appendix for discussion of each individual case.

2.2. *Data Reduction*

All of the observations were conducted in MIPS photometry mode. Most of the observations were conducted using the small-field photometry astronomical observing template (AOT) and, at 70 μm, the default pixel scale. For these targets (including those in the literature), we reprocessed the data in a uniform manner in order to limit systematics introduced by slightly different reduction methods. Two objects, η Tel and β Pic, were observed using observing strategies designed for extended objects (e.g., customized subpixel dithering and 70 μm fine scale). We note for completeness that while β Pic is well resolved at MIPS wavelengths, η Tel is not. Because these data must be handled differently anyway, rather than reprocessing the data, we use the MIPS photometry at 24 and 70 μm as reported by Su et al. (2006) for both η Tel and β Pic.

We started with the Spitzer Science Center (SSC) pipeline-produced basic calibrated data (BCDs), version S14. (For a description of the pipeline, see Gordon et al. 2005.) Since we treated each MIPS channel differently, each is discussed separately below.

Our detections and upper limits are listed in Table 3. Note that while every target was detected at 24 μm, one target was not observed at 70 μm (CPD -64 120), and more than half the sample was not observed at 160 μm. For most of our sample, this is the first time that MIPS fluxes have appeared in the literature. For the four FEPS stars that are part of the FEPS final delivery catalog (available on the SSC Web site) and for the three stars reported in Chen et al. (2005b) our fluxes are consistent within the reported errors.

2.2.1. 24 μm

All targets were observed at 24 μm. For each observation, we constructed a 24 μm mosaic from the pipeline BCDs using the SSC mosaicking and point-source extraction (MOPEX) software (Makovoz & Marleau 2005), with a pixel scale of $2.5''$ pixel^{-1}, close to the native pixel scale of $2.49'' \times 2.60''$. We extracted sources from the 24 μm mosaics using the astronomical point-source extraction (APEX) 1-frame portion of MOPEX, with point response function (PRF)-fitting photometry of the image mosaics. All of our targets were detected at good S/N (>25) at 24 μm. The systematic uncertainty in the zero point of the conversion from instrumental units to calibrated flux units is estimated to be 4% (Engelbracht et al. 2007); the statistical error is much smaller and so is not tabulated.

2.2.2. 70 μm

At 70 μm the SSC pipeline produces two sets of BCDs; in one the processing is done on the basis of individual BCDs, and the other has additional spatial and temporal filters applied that attempt to remove instrumental signatures in an automated fashion. (For a description of the pipeline, see Gordon et al. 2005.) We used the filtered BCDs to construct mosaics for all of the targets at 70 μm, resampled to $4''$ pixel^{-1}, about half the native pixel scale of $9.85'' \times 10.06''$.

We extracted sources from the 70 μm mosaics again using the APEX 1-frame portion of MOPEX. For the sources that were detected, most of the fluxes we report are from PRF-fitting; some bright source fluxes are better determined using aperture photometry instead. In those cases, an aperture of $32''$ and an aperture correction (multiplicative factor) of 1.295 was used. If no believable object was seen by eye at the expected location, it was taken to be a nondetection, and this aperture was laid down at the expected location of the target, plus two other nearby locations $\sim 1'$ north and south of the target position. Based on these measurements, an assessment of the 1 σ scatter per (native) pixel in nearby background sky brightness was made over the aperture, and that scatter was multiplied by 3 to obtain 3 σ upper limits. The same aperture correction was used as for the aperture photometry of detected objects.

All but one of the targets was observed at 70 μm. CPD -64 120 was not observed at 70 μm because its expected photospheric flux was far below the sensitivity that could be obtained in a reasonable amount of integration time. As can be seen in Table 3, 14 objects were detected and 24 were not detected (the 3 σ upper limits are in Table 3).

The systematic uncertainty in the conversion of instrumental units to calibrated flux units is estimated by Gordon et al. (2007) to be 5% for default-scale photometry. Gordon et al. are working with PSF fitting; we have some PSF fitting and some aperture photometry. In addition, some of our targets are fainter than the ones used in Gordon et al., and some of our targets are observed in fine-scale photometry mode. To be conservative, then, we take the systematic uncertainty to be 10%. Most of our objects are seen at S/N > 10; our statistical error on detections is much smaller than the systematic error of 10% in most cases, and so is not reported. In two cases, PZ Tel and ϵ Hya, the statistical error (as determined with similar methodology to that for the upper limits discussed above) is comparable to the systematic error. PZ Tel is detected with a S/N of $\sim$10 (uncertainty of 2 mJy on the 17.4 mJy detection in Table 3), and ϵ Hya is detected with a S/N of $\sim$3 (uncertainty of 4 mJy on the 12.6 mJy detection in Table 3).

Several of our targets have serendipitously imaged detections in the $5' \times 2.5'$ field of view (see Appendix A). The density of extragalactic background objects with brightness $\geq$15 mJy (the faintest 70 μm detection of a BPMG object achieved in this study) is 0.02 arcmin^{-2} (Dole et al. 2004). This leads to an expectation of 10 unrelated background objects appearing in our data. However, these are easily distinguished from our target objects by their offset positions; the probability is <1% that a background object would be coincident with any of our targets (see, e.g., Smith et al. 2006).

2.2.3. 160 μm

Twelve targets were observed at 160 μm. This subset of 12 targets was not selected uniformly for observation at 160 μm. For the targets that were observed as part of program 102, those objects expected to be brightest and seen at 70 μm were selected for observation at 160 μm. For the objects taken from other programs, we have no way of reconstructing why these targets were selected for observation.

TABLE 3
RESULTS: MIPS FLUX DENSITIES

OBJECT	24 μm (mJy)[a]		70 μm (mJy)[b]		160 μm (mJy)[c]	
	Photospheric	Measured	Photospheric	Measured	Photospheric	Measured
HR 9	60	109[d]	7.0	61[d]	1.3	<27
HIP 10679	23	39[d]	2.7	43.0[d]	0.5	...
HD 14082	36	37	4.2	<18	0.8	...
AG Tri A	14	17	1.7	75.1[d]	0.3	<35
AG Tri B	7.2	7.1	0.9	<23	0.2	<35
HIP 12545	16	12	1.9	<25	0.4	<50
51 Eri	114	115	13.2	<23	2.5	...
GJ 3305	29	24	3.4	<23	0.6	...
HIP 23309	34	27	4.0	<24	0.8	...
GJ 3322 A/B	30	28	3.8	<39	0.7	...
HR 1817	79	79	9.2	44.7[d]	1.7	<77
β Pic[e]	280	7276[d]	32	12,990[d]	5.9	3646[d]
AO Men	15	15	1.7	<8	0.3	<28
V343 Nor A/B	34	34	4.0	<86	0.7	...
HR 6070	90	97	10.4	<77	1.9	...
V824 Ara A/B	100	97	11.9	<25	2.2	...
V824 Ara C	9.9	11	1.3	<25	0.2	...
HD 164249	32	76[d]	3.7	624[d]	0.7	104[d]
HR 6749/HR 6750	120	113	14.4	<27	2.7	...
HR 7012	130	766[d]	15.6	197[d]	2.9	...
CD -64 1208 A/B	35	30	4.2	<23	0.8	...
PZ Tel	21	21	2.5	17.4[d]	0.5	...
η Tel A/B[e]	70	382[d]	8.1	409[d]	1.5	68[d]
HD 181327	32	195[d]	3.7	1468[d]	0.7	658[d]
AT Mic A/B	118	116	14.9	<18	2.9	...
AU Mic	164	143	19.4	205[d]	3.7	168[d]
HD 199143 A/B	35	35	4.0	<22	0.8	<31
AZ Cap A/B	15	13	1.8	<12	0.3	...
WW PsA A	19	18	2.4	<27	0.5	...
WW PsA B	8.6	9.1	1.1	<27	0.2	...
HD 987	12	12	1.4	<21	0.3	...
HIP 3556	9.5	8.4	1.2	<16	0.2	...
CPD -64 120	6.1	4.9	0.7	...	0.1	...
HD 10472	17	26[d]	1.9	127[d]	0.4	...
HD 12894	49	46	5.8	<20	1.1	...
ϕ Eri	150	170	17.3	<17	3.2	...
GSC 8056-0482	11	9.0	1.3	<24	0.3	...
ϵ Hya	140	124	15.9	12.6	3.0	...
HR 7848	179	186	20.8	609[d]	3.9	...

[a] The systematic uncertainty on our 24 μm flux densities is estimated to be 4% (Engelbracht et al. 2007).
[b] The systematic uncertainty on our 70 μm flux densities is estimated to be 10% (Gordon et al. 2007; see also discussion in text). Upper limits quoted here are 3 σ.
[c] The systematic uncertainty on our 160 μm flux densities is estimated to be 12% (Stansberry et al. 2007). Upper limits quoted here are 3 σ.
[d] Infrared excess and inferred disk at this wavelength; see text for discussion as to how these disk candidates were selected.
[e] The 24 and 70 μm flux densities are from Su et al. (2006); see text.

The MIPS data analysis tool (DAT) software (ver. 3.06; Gordon et al. 2005) was used to calibrate the raw data ramp slopes, apply a flat-field correction, and mosaic the images in detector coordinates at an image scale of $8''$ pixel^{-1} (half the native plate scale of $15.96'' \times 18.04''$). The data were flux-calibrated using the standard conversion factor of 1050 mJy arcsec^{-2} (flux unit)$^{-1}$, with about 12% systematic uncertainty (Stansberry et al. 2007). For our oversampled image mosaics, this is equivalent to 269 mJy DN^{-1} in a pixel.

The MIPS 160 μm array suffers from a spectral leak that allows near-IR radiation to produce a ghost image adjacent to the true 160 μm source image for stellar (roughly Rayleigh-Jeans) sources. The leak is only bright enough to appear above the confusion noise for sources with $J \sim< 5.5$ (MIPS Data Handbook, ver. 3.2). Among our stars observed at 160 μm, three sources are brighter than this limit: β Pic, η Tel, and AU Mic. In the first source, the circumstellar 160 μm emission is considerably brighter than the leak, so no effort was made to subtract off the leak. In the latter two sources, the leak was subtracted using observations of a photospheric standard, Achernar, from the *Spitzer* archive (AORKEY 15572992), as a reference source. The subtraction procedure is to empirically determine the maximum normalization factor for the leak reference source, such that its subtraction from the science target does not produce noticeable residuals below the background level.

To estimate upper limits to the 160 μm source flux densities, we measured the rms background variation among four 7×7 pixel apertures offset $64''$ along the detector rows/columns from the expected source position. For this aperture size, the 1 σ equivalent noise was calculated as $\frac{1}{7}$ of the individual pixel rms, assuming that the errors combine in quadrature. This value was then converted to a limiting flux density and corrected for the finite

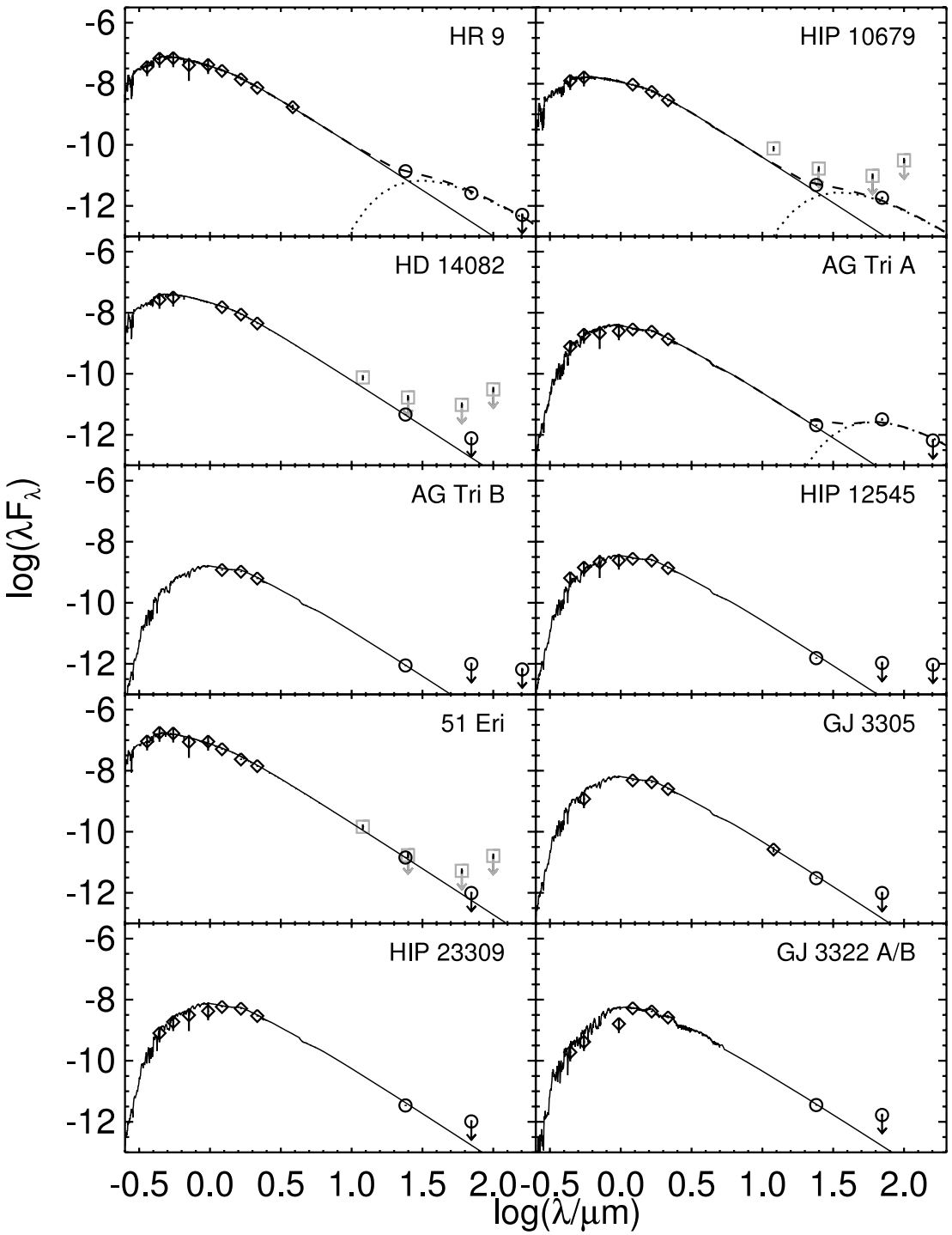

FIG. 1.—SEDs for all the BPMG targets discussed in § 1. The *x*-axis plots the log of the wavelength in microns, and the *y*-axis plots log (λF_λ) in cgs units (ergs s^{-1} cm^{-2}). Points gleaned from the literature are diamonds, boxes are detections or upper limits from *IRAS,* and circles are new MIPS points. Downward-pointing arrows indicate upper limits. The stellar model that is plotted is selected from the Kurucz-Lejeune grid (see text for discussion), normalized to the K_s band as observed; the simple disk model shown here is described in the text. The dotted line is the disk component alone, and the dashed line is the sum of the disk-plus-star model when more than one data point describes the disk.

aperture size using a multiplicative factor of 1.64 (measured from an STiny Tim model PSF; Krist 2005). Background cirrus emission can cause variation in the achieved sensitivity, with the 3 σ upper limits ranging over 27–77 mJy for our targets.

The five detections (and seven 3 σ upper limits) are listed in Table 3. Most of our objects are seen at S/N $>$ 8; our statistical error on detections is much smaller in most cases than the systematic error of 12%, and so is not reported. For η Tel, the detection has a S/N of $\sim$4 (error of 16 mJy on the 68 mJy reported in Table 3).

2.3. *Ancillary Data*

We consulted the literature for ancillary data on these objects, including spectral types, $UBVR_CI_CJHK_s$ and ground-based MIR magnitudes, distances, $v \sin i$, membership, etc. References consulted for literature values were the 2MASS (Skrutskie et al. 2006),

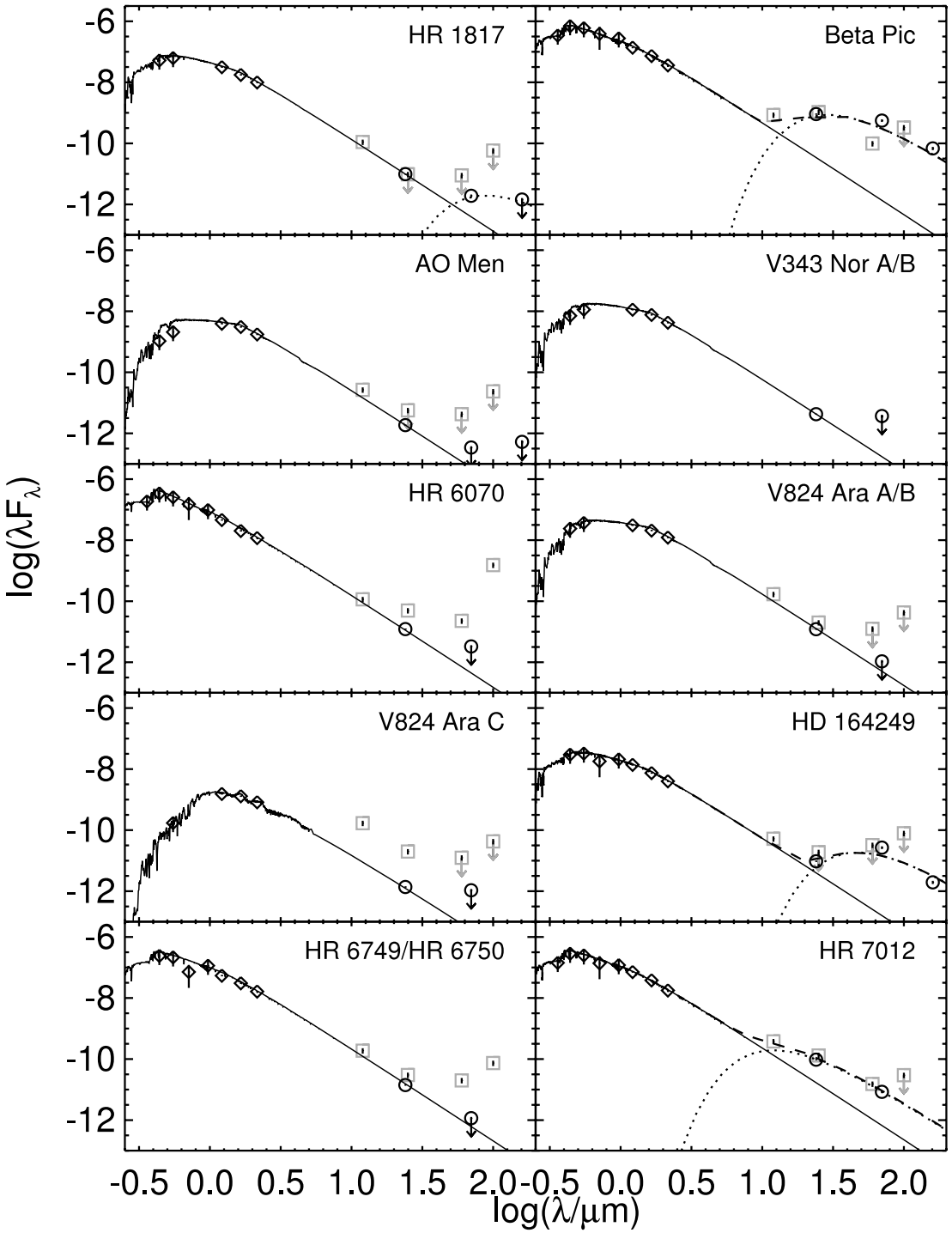

FIG. 2.—SEDs for all the BPMG targets discussed in § 2.

NASA Star and Exoplanet Database (NStED; Ali et al. 2005), the *IRAS* Faint Source Catalog (FSC; Moshir et al. 1992) and Bright Source Catalog (BSC; Beichman et al. 1988), as well as Zuckerman & Song (2004), Song et al. (2003), Feigelson et al. (2006), Chen et al. (2005b), Su et al. (2006), Kaisler et al. (2004), Zuckerman et al. (2001a, 2001b), Mamajek et al. (2004), Plavchan et al. (2005), Jayawardhana et al. (2006), and Schneider et al. (2006).

2.4. *SEDs and Expected Values*

Spectral energy distributions (SEDs) from U band through 160 μm, created from the literature data plus our MIPS fluxes, for all of these targets are portrayed in Figures 1–4. BPMG stars are in Figures 1–3, and Tuc-Hor stars are in Figure 4. Note that the error bars are usually smaller than the points; the points are hollow symbols, and the central vertical bar is the corresponding error.

If available, spectral types as determined from spectra (not from photometry) from the literature were used for each star. If no spectrum-based type was available, the type determined from $V - K$ color as reported in Zuckerman & Song (2004) was used; these types appear in Table 1 as types without luminosity classes. Using temperatures and gravities inferred from the spectral type, we selected the closest grid point from the Kurucz-Lejeune model grid (Lejeune et al. 1997, 1998). This stellar model is shown in

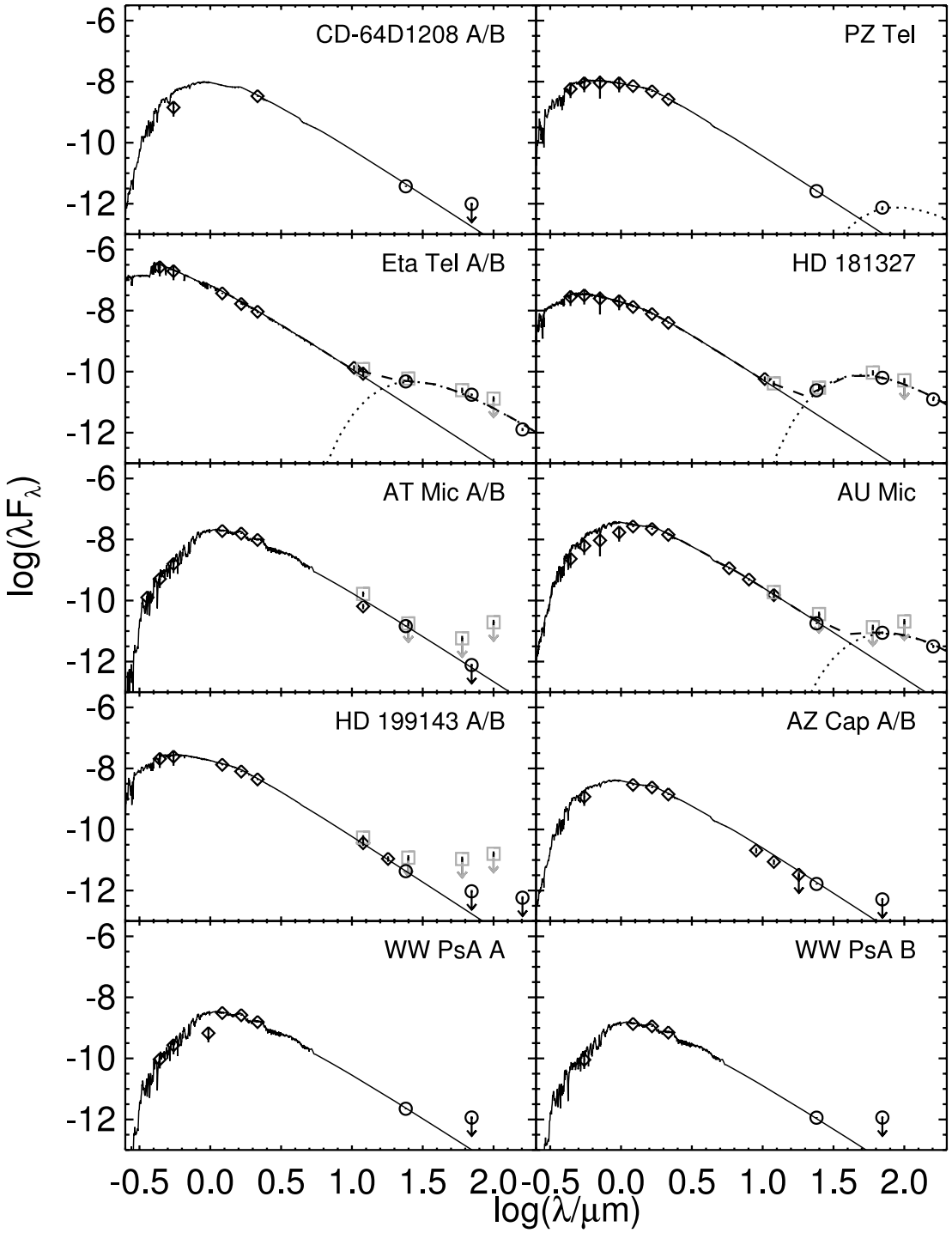

FIG. 3.—SEDs for all the BPMG targets discussed in § 3.

Figures 1–4 and is used to determine the expected photospheric flux densities for the sample of stars at MIPS wavelengths. The models are normalized to the observed data at K_s. Interpolating models, rather than selecting the nearest grid point, does not make any significant difference in the expected photospheric flux density. Using a single spectral type for unresolved binaries rather than a hybrid of two spectral types also does not make any significant difference in the expected photospheric flux density (see Trilling et al. 2007).

Because the spectral types are already well known for most of these stars, we did not wish to allow the spectral type to be a free parameter in our fits. However, we did wish to assess the goodness of the fit. Values of χ^2_ν were calculated for the models in Figures 1–4, and, as can be seen by eye in the figures, all the fits are quite good, even given occasional deviant optical points pulled from the literature. For most of the objects, typical values of χ^2_ν are $\sim$0.46 (e.g., typically $<$10% chance that the model is a bad fit). For the remaining objects, typically one optical point is off (e.g., GJ 3322 A/B; see Fig. 1), which distorts the χ^2_ν; dropping those points brings the χ^2_ν into line with the rest of the objects.

The expected photospheric flux densities were linearly interpolated to the MIPS wavelengths from the Kurucz-Lejeune model. These estimated photospheric flux densities are included in Table 3. If the assumed spectral type is off by a subclass, over the entire

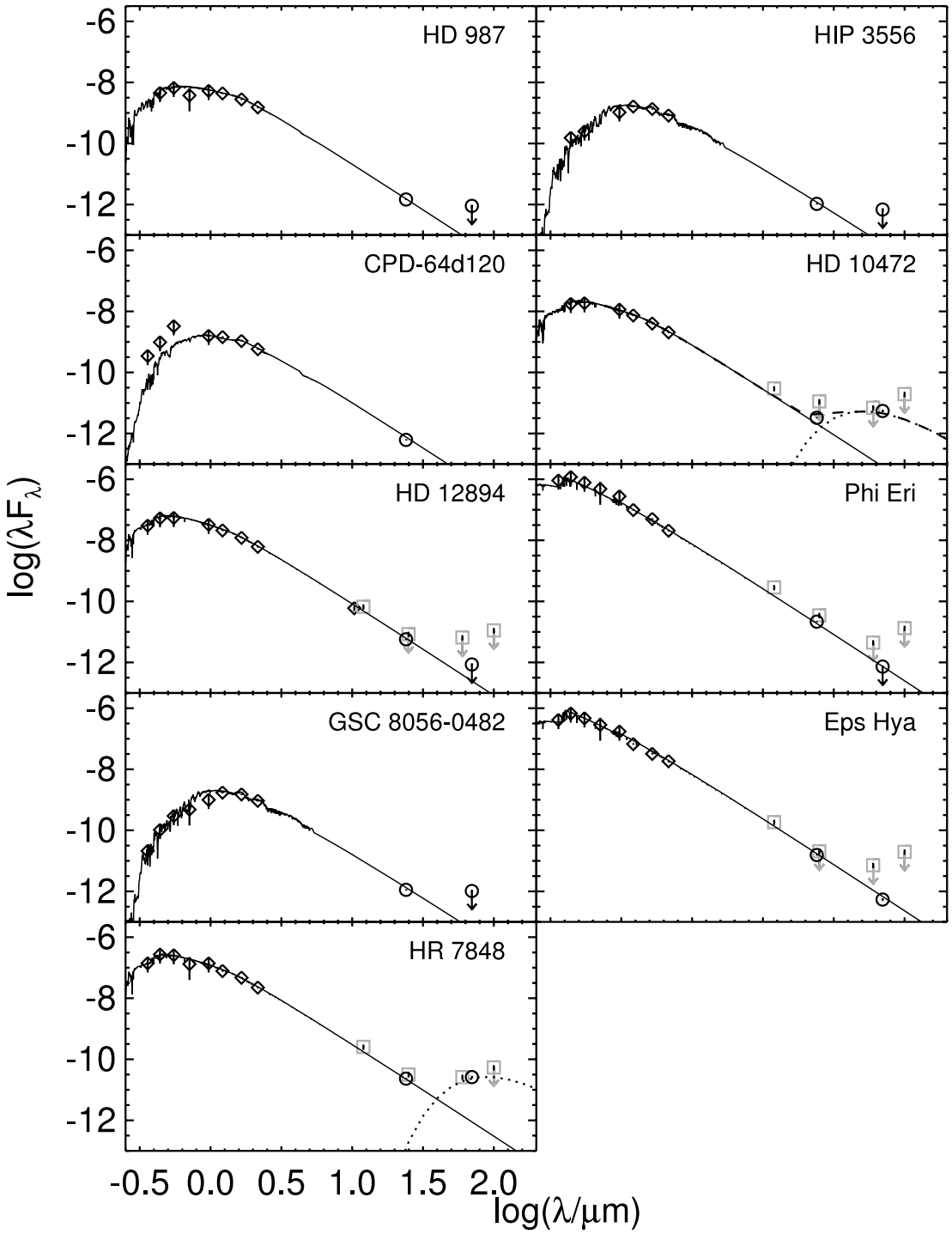

FIG. 4.—SEDs for all the Tuc-Hor targets discussed in this paper. Notation is as in previous plots.

range of types considered in this paper, there is typically a $\lesssim$4% change in the calculated photospheric flux, comparable to the systematic uncertainty in the measured 24 μm fluxes.

3. RESULTS: INFRARED EXCESSES IN THE BPMG

3.1. *Excesses at* 24 μm

There are a variety of methods in the literature for finding circumstellar disks based on the 24 μm excess. We consider a few slightly different methods here and establish our final sample of seven objects (plus one more from Tuc-Hor) with excesses at 24 μm.

Figure 5 is a color-magnitude diagram of K_s vs. $K_s - [24]$. In this figure, four stars stand out obviously as having $K_s - [24] > 1.5$: β Pic, HR 7012, η Tel, and HD 181327. We could declare these four stars as our only stars with excesses. However, more subtle excesses are certainly present in the remaining stars; the points do not scatter evenly around $K_s - [24] = 0$. Even omitting the *five* stars with the largest $K_s - [24]$, the mean $K_s - [24]$ color is 0.23, although there is a large standard deviation; the 1 σ dispersion is 0.25.

To identify which of the remaining stars have excesses, we consider the photospheric color. For most spectral types, the photospheric $K_s - [24]$ color should be close to 0. Gautier et al. (2007)

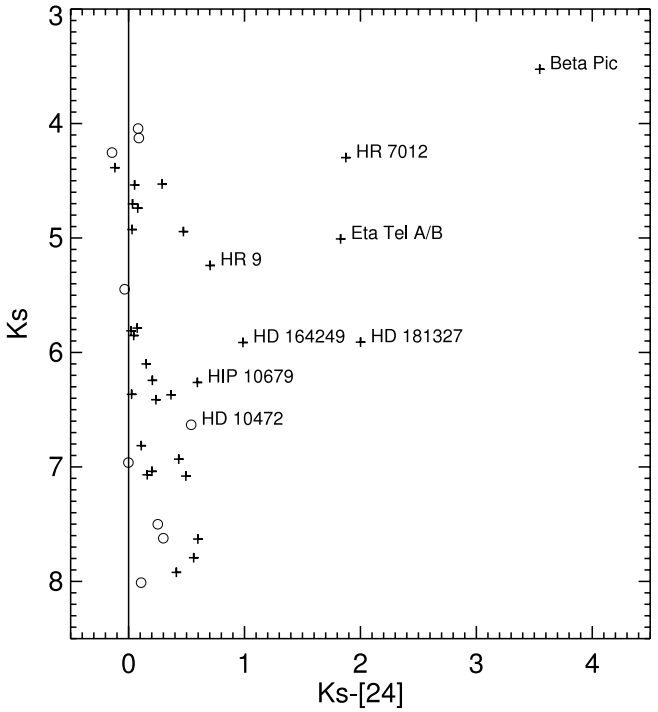

FIG. 5.—Plot of K_s vs. $K_s - [24]$ for all of the objects considered here. Plus signs are objects from the BPMG; circles are objects from Tuc-Hor. The objects with excesses at 24 μm, selected by a combination of techniques, are indicated by name; see text for discussion as to how the objects with excesses were selected.

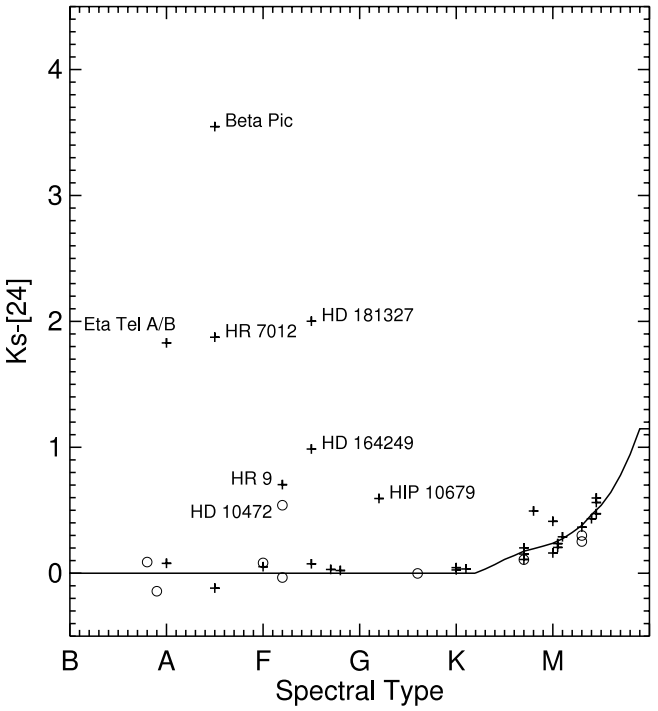

FIG. 6.—Same as Fig. 5, but for $K_s - [24]$ vs. spectral type. The solid line indicates expected photospheric color (Gautier et al. 2007).

find for M stars that there is a dependence of $K_s - [24]$ color with $T_{\rm eff}$ such that the latest types have a $K_s - [24]$ color up to 1.5 for the coolest stars considered there ($T_{\rm eff} \sim 2000$). Figure 6 shows the $K_s - [24]$ color as a function of spectral type for our sample here, along with the photospheric line from Gautier et al. (2007). The nonzero color for the latest types is readily apparent, and the tightness of the correlation as a function of spectral type through the Ms clearly follows the photospheres (see Gautier et al. 2007 for more discussion). For types earlier than K0, we have another four stars whose $K_s - [24]$ colors are clearly distinct from 0: HD 164249 (F5), HR 9 (F2), HIP 10679 (G2), and HD 10472 (F2). These objects too are therefore likely to possess excesses at 24 μm.

We clearly need to take into account expected photospheric flux to assess the significance of the $K_s - [24]$ excess, and for that we need to depend on a model estimate of the photospheric flux. Bryden et al. (2006) consider nearby solar-type stars, calculating the ratio of the measured to expected fluxes at 24 μm. They determined infrared excess objects to be those with $F_{\rm meas}/F_{\rm pred} > 1.2$. Taking $F_{\rm meas}/F_{\rm pred} > 1.2$ provides a relatively conservative disk criterion at 24 μm, in that it sets a limit that is more than 3 times the systematic error of 4%, also providing ample room for the comparable $\sim$4% uncertainty in the calculation of $F_{\rm pred}$. In our sample, we can construct a (sparse) histogram of $F_{\rm meas}/F_{\rm pred}$, and, as expected, the histogram is sharply peaked around 1 with a break at 1.2 and a long tail extending out to $\sim$27.[6] The 1 σ scatter in the points centered on $F_{\rm meas}/F_{\rm pred} \sim 1$ is 0.09. The similar analysis in Bryden et al. (2006) finds a 1 σ scatter of 0.06. The number we obtain, 0.09, is an upper limit to the true error because we have fewer stars than Bryden et al. and are using different methodology (normalizing the star to K_s rather than fitting to the entire SED); a few stars in our sample could inflate the error as a result of small excesses or incorrect K_s magnitudes. On this basis, we believe our results to be fundamentally consistent with those from Bryden et al. (2006).

The eight objects identified above have $F_{\rm meas}/F_{\rm pred} > 1.2$. Note that β Pic itself has a ratio of $\sim$27 (the largest of the sample). As shown in Figure 6, HD 10472 has the smallest ratio, 1.6. Assuming our scatter above of 0.09 as the worst-case scenario, this lowest excess of our entire data set is a 6 σ excess.

There are two M stars in Figure 6 that could have slight excesses, as their $K_s - [24]$ are redder than other objects of similar spectral type; they are AG Tri A and B. AG Tri A has a ratio that is exactly 1.2. AG Tri A will emerge in the next section as having a 70 μm excess, so it is quite possible that it has a small 24 μm excess. AG Tri B has only a slightly larger $K_s - [24]$ than other stars plotted of similar spectral type and has $F_{\rm meas}/F_{\rm pred}$ at 24 μm of 0.98, well below our adopted excess criterion.

AU Mic is known to have a resolved disk at other wavelengths (e.g., Graham et al. 2007), so we investigated the evidence for an infrared excess more closely. The spectral type of this star is usually taken to be M1 (e.g., Graham et al. 2007; Houk et al. 1982); it has $K_s - [24] = 0.29$, which is comparable to the photospheric emission from other stars of that spectral type from Gautier et al. (2007). AU Mic has $F_{\rm meas}/F_{\rm pred}$ at 24 μm of 0.9, if anything suggestive of a flux deficit at 24 μm. If the spectral type of AU Mic were incorrect, and its true spectral type was earlier, our analysis method would yield a smaller value of $F_{\rm pred}$ and hence a larger value of $F_{\rm meas}/F_{\rm pred}$. In order to yield $F_{\rm meas}/F_{\rm pred} > 1.2$, however, the true spectral type would have to be early K. We have obtained our own high-S/N, echelle spectrum of AU Mic in order to constrain better its spectral type (J. R. Stauffer et al. 2008, in preparation). Based on the strength of the TiO band heads near 7050 Å, we estimate a spectral type at least as late as M1, and exclude a spectral type earlier than M0. Therefore, we believe our determination that AU Mic does not have an excess at 24 μm is robust. In support of this, we note that the IRAS 25 μm flux is

[6] To see the distribution of $F_{\rm meas}/F_{\rm pred}$ in one dimension, see Fig. 11.

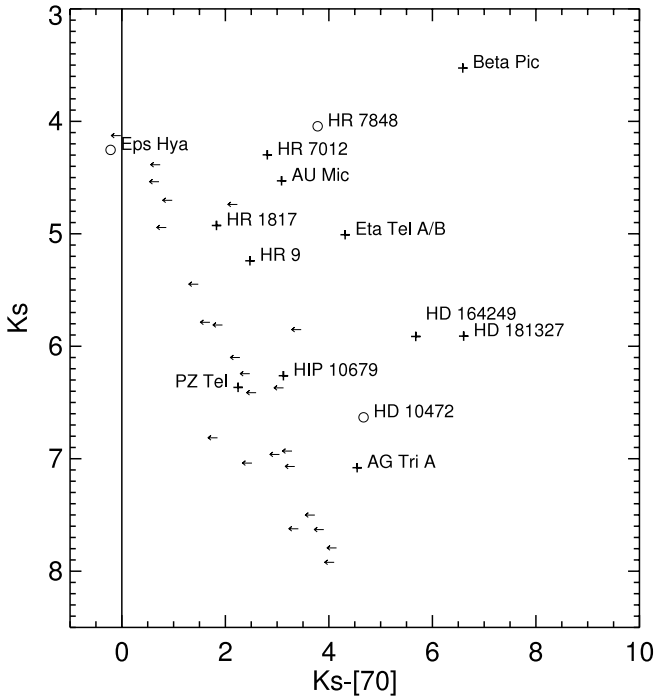

FIG. 7.—Plot of K_s vs. $K_s - [70]$ for all of the objects considered here. Plus signs are detected objects from the BPMG; open circles are detected objects from Tuc-Hor. All other objects (from both associations) are indicated as upper limits at 70 μm. All detections except ϵ Hya suggest excesses at 70 μm.

comparable to our 24 μm flux and that Chen et al. (2005b) also conclude that the star has no 24 μm excess.

Formally adopting the Bryden et al. (2006) criterion, then, we find that 8 out of the 39 stars or star systems in our entire sample have 24 μm excesses. Out of the 30 stars in the BPMG for which we have measurements, 7 have $F_{\rm meas}/F_{\rm pred} > 1.2$. Assuming that the excesses are due to circumstellar disks, this implies a disk fraction at 24 μm of 23%.

3.2. *Excesses at* 70 μm

Figure 7 shows a plot similar to Figure 5 but for $K_s - [70]$ colors. Here expected photospheric colors are $K_s - [70] \sim 0$. Bryden et al. (2006) set a value of $F_{\rm meas}/F_{\rm pred} \gtrsim 2$ (the precise level is dependent on the background level) to divide the disks from the nondisked stars. The overall scatter found for the Bryden et al. $F_{\rm meas}/F_{\rm pred}$ for stars without excesses was 25%, so the limit of $F_{\rm meas}/F_{\rm pred} \gtrsim 2$ corresponds to 4 σ.

In our data, just 14 stars are detected at 70 μm (compared with 39 stars detected at 24 μm). We have many fewer detections than Bryden et al. (2006), and even on initial inspection of the SEDs or Figure 7, just one object (ϵ Hya) seems to be a likely photospheric detection. In the 24 μm section above, we were able to examine the scatter of our measurements of $F_{\rm meas}/F_{\rm pred}$ for photospheres in our sample; there is no way for us to repeat this analysis here at 70 μm as a check on the $F_{\rm meas}/F_{\rm pred} \gtrsim 2$ excess cutoff. However, all of the detections at 70 μm are clear excesses, with the exception of ϵ Hya. ϵ Hya has $F_{\rm meas}/F_{\rm pred} < 0.8$, and all the rest of the detections are $F_{\rm meas}/F_{\rm pred} > 4.9$, well beyond the Bryden et al. limit (20 σ, assuming the 0.25 scatter), so we believe that the exact value for the criterion to separate stars with excesses from those without is not critical. AG Tri A, which was determined above to have an insignificant 24 μm excess, has $F_{\rm meas}/F_{\rm pred} = 44$ at 70 μm.

Fourteen of our larger sample of 38 stars or star systems are detected at 70 μm. The sensitivity of the 70 μm observations in this sample varies considerably because of the range of exposure times used in these observations and the cirrus background. Out of the 30 members of the BPMG, 11 are detected, all of which have considerably more than photospheric emission. This represents a lower limit on the BPMG excess fraction (at 70 μm) of 37%.

3.3. *Excesses at* 160 μm

None of the observations at 160 μm are sensitive enough to detect the expected photospheric flux densities, so all of the 160 μm detections are suggestive of excesses. Of the 12 BPMG stars with 160 μm data, 5 are detected (β Pic, HD 164249, η Tel, HD 181327, and AU Mic). Because the sample of stars selected for observation at 160 μm is biased toward those with disks, we cannot infer a limit on the excess fraction (at 160 μm).

All stars detected at 160 μm are also detected at 70 and 24 μm, and almost all of the stars with 160 μm excesses also have excesses at the other two MIPS wavelengths. The sole exception is AU Mic, which has a clear excess at 70 but not at 24 μm. Based on the blackbody fits (see below), in no case does the 160 μm detection suggest a cold component of dust that is not seen at the shorter MIPS wavelength(s). (For a discussion of how much cold dust could be included within the uncertainty of the 160 μm detections that is not already accounted for with the component seen at 24 and 70 μm, please see Gautier et al. 2007.)

3.4. *Comparison with IRAS*

Of our 39 targets observed at 24 μm from both the BPMG and Tuc-Hor, 19 appear in the *IRAS* FSC or BSC with either detections or upper limits (plus 3 more included with a nearby association member by the *IRAS* beam). Discussion of individual objects is in Appendix A, including those objects where MIPS observations have resolved source confusion (or background contamination) found in the large-beam *IRAS* measurements.

In summary, the MIPS observations confirm five excesses discovered by *IRAS*. In 5 more cases (four of which have excesses at 70 μm), MIPS provides a detection near the *IRAS* limit. For the remaining 9 systems, MIPS establishes a new much more stringent upper limit on any excess that may be present; at least 3 of those previously appeared to have an excess based solely on *IRAS* results. There are three new excesses without any prior IRAS detections or limits. For individual source assessment, the SEDs for each object (including *IRAS* detections and limits) appear in Figures 1–4, and discussion of specific cases appears in the Appendix.

4. DISK PROPERTIES

We note here for completeness the following items. Simply having $L_{\rm dust}/L_* < 1$ does not assure that the disk is really a debris disk, which by definition requires a second generation of dust and gas depletion; however, values of $L_{\rm dust}/L_* \sim 10^{-3}$ are likely debris disks. *Spitzer* MIPS observations constrain the presence of dust in these systems, but say nothing about any gas or grains much larger than the wavelength of observation. From this point forward, we have assumed that any excess infrared emission that we observe above the photosphere is due entirely to a dusty circumstellar disk. Until observations at any wavelength resolve the disk, this remains an assumption.

4.1. *Blackbody Fits*

For those 13 objects that we find to have excesses at any MIPS wavelength, Figures 1–4 show a fit to the star+disk SED. The excesses are modeled as simple blackbodies, which we use for an

TABLE 4
MODEL RESULTS: DISK PROPERTIES

Object	Simple Blackbody Models				More Complex Models		
	BB T (K)	L_{dust}/L_* ($\times 10^{-5}$)	Min. R_{dust} (AU)	Min. M_{dust} (M_{moon})	M_d (M_{moon})	R_i (AU)	R_o (AU)
Disks Detected at More than One Wavelength							
HR 9	120	10	10	0.0004	0.25	35	200
HIP 10679	100	80	20	0.01	0.4	35	200
AG Tri A[a]	65	79	10	0.003	...[c]	...	...
β Pic[b]	130	180	10	0.012	...	...	...
HD 164249	78	59	20	0.01	...[c]	...	...
HR 7012	310	90	2	0.0002	0.05	5	200
η Tel A/B	140	24	20	0.0027	0.8	70	200
HD 181327	75	250	20	0.06	10	68[d]	104[d]
AU Mic	50	23	8	0.0005	1	35	200
HD 10472 (Tuc-Hor)	70	67	30	0.02	30	400	700
Disks Detected Only at 70 μm							
HR 1817	(41)	>3.0	(60)	(0.004)	0.3	100	200
PZ Tel	(41)	>7.3	(50)	(0.006)	0.3	35	200
HR 7848 (Tuc-Hor)	(41)	>13	(100)	(0.07)	5	250	400

[a] Since the F_{meas}/F_{pred} at 24 μm for this star was right at 1.2, we attempted modeling of this star including the observed flux density at 24 μm.
[b] A simple disk fit was made for β Pic for self-consistency with the rest of the sample; this object is resolved at MIPS wavelengths and the disk is better characterized using other methods.
[c] No fit possible; see text for discussion.
[d] Inner and outer radii are fixed at the values reported by Schneider et al. (2006).

initial simple characterization of the disks, akin to an assumption of a single-temperature thin ring of dust.

In three cases (HR 1817, PZ Tel, HR 7848), we have a single data point at 70 μm that describes the disk excess. For these objects, we follow the example set by Bryden et al. (2006) and simply set the peak of the blackbody to be at 70 μm (41 K for λF_λ). In 10 cases, we have more data (detections and limits) that describe the disk; for these stars, we have found the best-fit blackbody by χ^2 minimization analysis, allowing the best-fit blackbody to run through the upper limits where available. The temperatures corresponding to those fits can be found in Table 4. Note that in the case of AG Tri A, the F_{meas}/F_{pred} at 24 μm is 1.2, so a small excess at 24 μm cannot be ruled out; we modeled this star including this potentially small excess at 24 μm, so it is effectively treated as a star with more than one disk detection.

Since a blackbody has two free parameters, disks with two data points describing the disk are fit perfectly by a blackbody, and this can clearly be seen in Figures 1–4. We do not expect a simple blackbody to be a good fit to disks with three data points, because in reality there is wavelength-dependent grain emissivity for small grains that is not accounted for in a simple blackbody, and there is likely to be dust with a range of temperatures. Clearly, better models than a simple blackbody are needed to characterize the disks (see below). Nonetheless, as can be seen in Figures 1–4, the fits are acceptable for even the four objects (β Pic, HD 164249, η Tel, and HD 181327) with excesses at all three MIPS bands, although, not surprisingly, many are not within 1 σ of the data points. The fit for HD 164249 is the most discrepant, running below the 70 μm point (333 mJy predicted by the model, compared to 624 mJy observed) but above the 160 μm point (170 mJy predicted vs. 104 mJy observed). In this case in particular, the dust distribution may well be impossible to characterize with a single-temperature simple blackbody, even with grain emissivity included—for example, there may be a range of particle sizes and a large distribution of orbital radii. Indeed, spectral features have been resolved from disks around β Pic, HR 7012, and η Tel (Chen et al. 2006, 2007). Nevertheless, for completeness and self-consistency within the sample, we list the numbers obtained via the simple blackbody fit in Table 4.

The hottest dust found in the sample is $\sim$300 K for HR 7012. AU Mic's disk, which is resolved by other instruments (e.g., Kalas et al. 2004; Krist et al. 2005), although not by MIPS (Chen et al. 2005b), is fit by the coldest dust of any of these objects (especially among those with 160 μm detections) at $\sim$50 K, which is consistent with a disk excess at 70 and 160 but not 24 μm.

Although we also fit β Pic, AU Mic, and HD 181327 with single blackbodies for self-consistency within the sample, and, for comparison here, we note that these objects are resolved at other wavelengths—β Pic is resolved even at MIPS wavelengths (Su et al. 2004) and is known to not be a single-temperature narrow ring—so their disks are better characterized using other methods that take into account that spatial information.

4.2. *Fractional IR Excess*

Since we have a wide range of spectral types represented in this association, we would like to use a measurement of the disk luminosity that attempts to compensate for the central star's luminosity. We used the fits described above to derive a value for the fractional disk luminosity, L_{dust}/L_*; these values appear in Table 4. To determine L_{dust} for stars which have an excess described by more than one detection, we integrate under the disk model fit, having subtracted off the photospheric contribution. In order to determine the L_{dust}/L_* value for stars whose excesses are only observed at 70 μm, we follow Bryden et al. (2006, eq. [3]), determining the minimum L_{dust}/L_* by assuming that the blackbody continuum peaks at 70 μm.

The L_{dust}/L_* values that appear in Table 4 for disks detected in more than one wavelength range from 10^{-4} to 2.5×10^{-3}, with a median value of 7.9×10^{-4}.

4.3. *Minimum Radius and Minimum Mass*

Assuming that the grains composing the disks are in thermal equilibrium, we can follow a similar analysis as that found in Low et al. (2005) or Smith et al. (2006) to determine a minimum radius and minimum mass of the disk. We assume blackbody dust grains in thermal equilibrium with the stellar radiation field and constrain the inner radius of the disk along with a minimum mass of the disk. Following Low et al. (2005), we use the relationship from Chen & Jura (2001). We assume the same values for average grain size (2.8 μm) and density (2.5 g cm^{-3}) adopted there (and in Low et al. 2005 and Smith et al. 2006), despite the fact that these parameters, having been derived for ζ Lep (an A3 star), may be more appropriate for much more massive stars than we have here on average (see additional discussion below). Values of minimum radius and minimum mass so calculated appear in Table 4. For disks detected in more than one wavelength, the minimum radius ranges from 2 to 30 AU, and the minimum mass ranges from $\sim$0.0002 to $\sim$0.06 $M_{\rm moon}$.

4.4. *Literature Models*

Spitzer Infrared Spectrograph (IRS; Houck et al. 2004) observations of HD 181327, HR 7012, and η Tel were discussed and modeled in Chen et al. (2006). The IRS observations extend to 33 μm. The MIPS 24 μm flux densities are consistent with the IRS spectra; since the Chen et al. (2006) models were designed to fit IRS spectra between 4 and 33 μm, of course the models are also, by construction, consistent with our MIPS 24 μm flux densities. In all three cases, these models can be extended past 33 μm to predict flux densities at 70 and 160 μm, and they are found to be in very good agreement with the observed flux densities.

For HD 181327, the IRS spectrum is featureless and Chen et al. model the excess as a simple blackbody, making it straightforward to compare their model parameters to ours. The blackbody temperature from Chen et al. is 81 K; our blackbody temperature is 75 K, which we consider to be identical to within the errors. The $L_{\rm dust}/L_*$ reported by Chen et al. is 3.1×10^{-3}, to be compared with 2.5×10^{-3} derived here. The minimum mass of the disk is 4×10^{24} grams in this paper and 1×10^{24} grams in Chen et al. The Chen et al. model predicts a 70 μm flux density of 1.2 Jy (20% different than observations) and a 160 μm flux density of 0.62 Jy (3% different than observations).

For the other two stars (HR 7012 and η Tel), Chen et al. found features in the IRS spectra and constructed much more detailed, multicomponent models (with various mineral species and a range of grain sizes, etc.), making comparison to parameters derived from our single-component blackbody fits relatively unilluminating. However, in order to match the overall structure of the IRS spectra found near $\sim$30 μm, Chen et al. required a cooler component, up to two blackbodies of different temperatures and total solid angles. The assumptions of the models are sufficiently different from ours as to make simple comparisons difficult. These differences simply illustrate the latitude even relatively detailed models have in fitting the existing data, given the large number of parameters that can be adjusted. The one somewhat meaningful comparison is of the blackbody temperatures to fit the longest wavelength flux densities. For HR 7012, Chen et al. adopted a blackbody temperature of 200 K, versus 310 K for our models; for η Tel, Chen et al. adopted two blackbodies, one of 115 K and the other of 370 K (however, the total solid angle of the 115 K component was much larger), versus our 140 K single blackbody. For HR 7012, the predicted flux densities are 0.27 and 0.072 Jy at 70 and 160 μm, respectively; at 70 μm, the observed flux density is 35% different from the model, and it was not observed at 160 μm. For η Tel, the Chen et al. predicted flux densities are 0.39 and 0.14 Jy, and our observed values are just 5% and 8% different from the model.

4.5. *New Models*

Thirteen of the 40 targets have flux excesses above photospheric levels in at least one of the MIPS bands. Of these, β Pic itself has been studied extensively in the literature (most recently Chen et al. 2007), and we consider it no further here. We have fit the data points as portrayed in Figures 1–4 for the remaining 12 systems using continuum spectra computed in each case for an axisymmetric and optically thin disk of astronomical silicate grains in radiative equilibrium with the stellar field. The models are described further in V. G. Mannings et al. (2008, in preparation); below, we summarize the characteristics of the models.

4.5.1. *Model Description*

We assume grain radii distributed as a power law from 0.001 μm to 1 mm. The index of the *continuous* power-law distribution in grain size is here fixed at -2.5, leading directly from the index of -3.5 for the number of grains *per unit size interval* described in the classic study of interstellar grains by Mathis et al. (1977). Optical constants are taken from B. Draine for the smaller grains.[7] We compute absorption efficiencies for the larger grains by modifying the Mie code developed by Bohren & Huffman (1983). We then distribute the grains across a disk geometry assuming a surface density viewed normal to the disk plane that falls off as a power law from an inner disk radius R_i to an outer radius, R_o. (See Sylvester & Skinner 1996 for similar modeling of debris disks.) The power-law index for the radial density distribution is held at the typical value of -1.5 assumed for circumstellar disks (e.g., Kenyon & Bromley 2002). The disk inclination angle is irrelevant for optically thin emission, as is the (likely) nonzero opening angle of the disk as viewed from the star. The remaining disk parameter is simply the total mass of grains, M_d. To limit the number of free parameters (since in several cases we have but one point defining the disk), we fix all quantities with the exception of R_i, R_o, and M_d. These three parameters dominate in different wavelength regimes, so we are able to hone in on a unique fit despite the sparseness of the data. To first order, the value of R_i establishes, for a fixed range of grain sizes, as in this model, the wavelength at which the disk spectrum exhibits a peak, while M_d determines the luminosity of the disk. The spectrum is relatively insensitive to R_o. Increasing the value of R_o relative to R_i is akin to spreading the grains out to greater distances from the star, but since the radial density falls as a power law, the effect on the total spectrum is marginal. It can be perceived as a gentle softening of the ratio of the total flux emitted by warm grains (inner disk) and cool grains (outer disk). We show our model SEDs in Figure 8.

4.5.2. *Model Results and Comparison*

The best-fit values are listed in Table 4 for M_d, R_i, and R_o, as derived using these models and the optical+near-IR+MIPS data that appear in Figures 1–4. Disk masses range from about 0.05 to 30 $M_{\rm moon}$. Disk inner radii take values from 5 to 400 AU, and outer radii range from about 100 to 700 AU. The median fractional difference between the model and the observations at 24 μm is -0.12, including the value from HD 181327, which is the most discrepant, at 24 μm (see Fig. 8 and discussion below). The closest fit is HIP 10679, where the model matches the observations to

[7] At http://www.astro.princeton.edu/~draine.

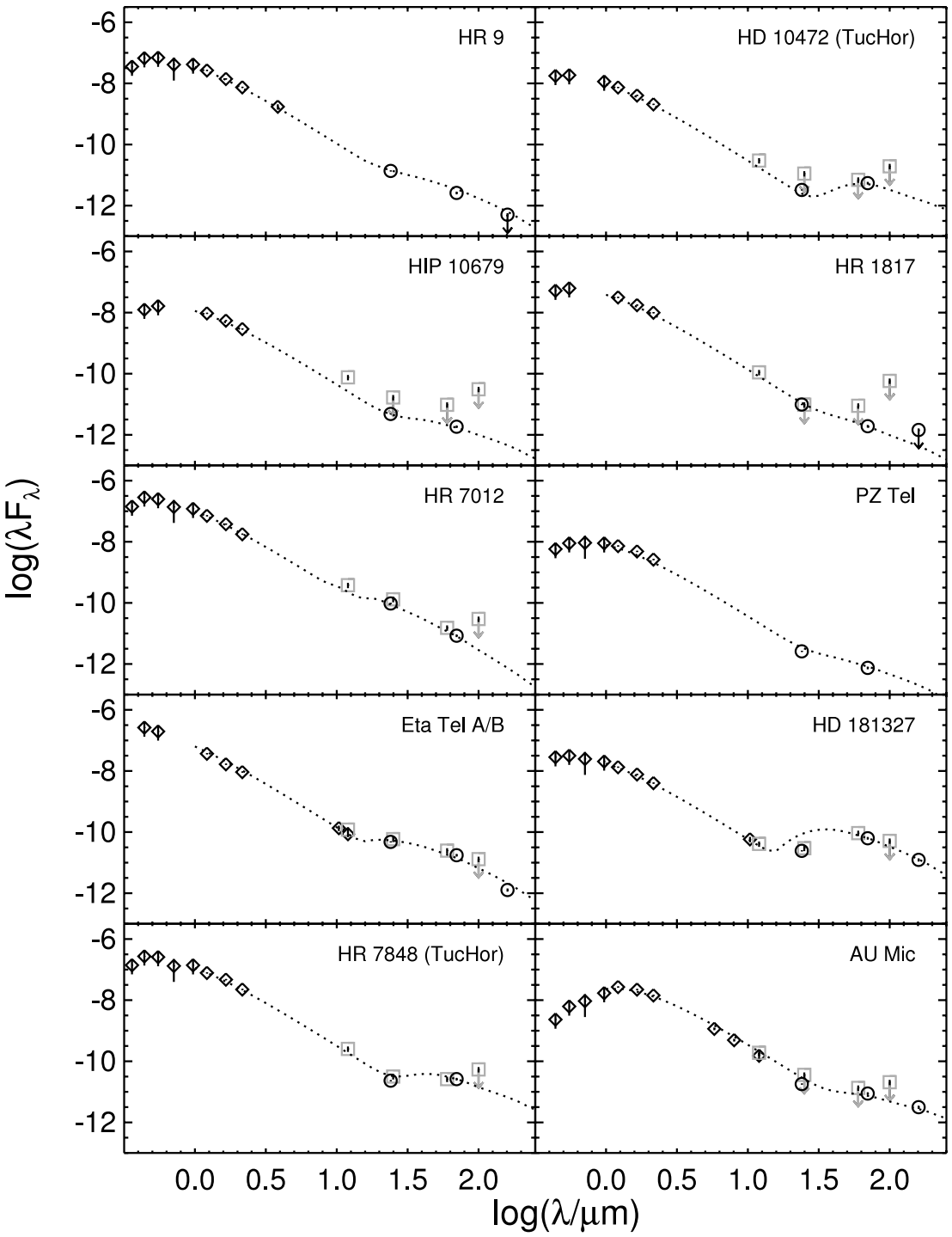

FIG. 8.—Star+disk models of the 10 stars considered for more sophisticated modeling; see text for discussion as to how they were selected and the details of the modeling. Notation is as in Figs. 1–4: the x-axis plots the log of the wavelength in microns, and the y-axis plots log (λF_λ) in cgs units (ergs s^{-1} cm^{-2}). Points gleaned from the literature are diamonds, boxes are detections or upper limits from *IRAS*, and circles are new MIPS points. Downward-pointing arrows indicate upper limits.

3%. Given that the systematic uncertainty of our 24 μm observations is 4%, the model is then typically $\sim$3 times off at 24 μm. At both 70 and 160 μm, the median fractional difference between the model and observations is just 0.04, well within the systematic uncertainty at either band.

The simpler models calculated following Low et al. (2005) in § 4.3 (hereafter abbreviated as model 1), not surprisingly, produce much different values of disk masses and radii than those calculated here. The models from Mannings et al. (hereafter abbreviated model 2) are more complex; both models 1 and 2 are physically valid within the limitations of their own set of assumptions, which we now discuss.

Model 1, in order to calculate the minimum disk mass and inner minimum disk radius, must make simple assumptions about the grain size (2.8 μm) and density (2.5 g cm^{-3}), and assume that the grains radiate as blackbodies. These assumptions trace back to Chen & Jura (2001), who studied an A3 star, ζ Lep; they took 2.8 μm for grain size because grains smaller than this would be ejected from the system due to radiation pressure. This is *not* a universally valid assumption for these BPMG stars (or for that

matter for the TWA stars from Low et al. 2005), because there are much cooler M stars included in both the BPMG and TWA. But such calculations nonetheless serve to provide a rough comparison between star-disk systems across papers and associations.

Model 2 obtains such different results for disk masses and sizes for a variety of reasons, all traced back to grain size and location assumptions. Model 2 assumes that each disk is a power-law mixture of grain sizes (from ISM size to 1 mm), and that the mixture is spread out across the disk (not in a thin ring). Most of the grains are a factor of 3000 smaller in radius than that assumed in model 1, and the grain emission is not blackbody. Small nonblackbody grains tend to be hotter than larger (e.g., blackbody) grains at the same distance from a star, so the small grains must be further out to get lower temperatures and, therefore, similar fluxes. That in part accounts for the model 2 disk inner radii being larger than those of model 1. (Moreover, the radii from model 1 are artificially reduced by the assumption that the particles radiate like blackbodies at the temperatures or wavelengths of interest, which is almost certainly not the case, as even 3 μm particles are small compared to the relevant wavelengths.) Because model 2 has larger disk radii, a much larger amount of dust area is needed to subtend a given solid angle to absorb the stellar light and match the observations. The model 2 disk masses are larger than those of model 1 for two reasons. First, because the best-fit inner disk radii are larger than the model 1 values, a greater amount of integrated grain surface area is needed in model 2 to subtend a similar total solid angle, as viewed from the star, to that for model 1. Second, due to the power-law distribution in grain sizes, a significant amount of disk mass is locked up in the large end of the size range, while the absorption and reemission of starlight is dominated by grains at the small end. The small grains contribute negligibly to the disk mass, but they dominate the radiative transfer and, therefore, the output spectrum.

4.5.3. *Notes on Models of Specific Sources*

For HD 181327, the inner and outer radii were fixed at the values reported by Schneider et al. (2006), despite the fact that those parameters were obtained from wavelengths shorter than 24 μm. Only the mass was left as a free parameter in our model fit. This (plus the other constraints imposed) explains why the predicted model flux density at 24 μm is so different from the observed flux density (see Fig. 8 and below).

Two of the 12 sources with flux excesses cannot be fit with model disk spectra: AG Tri A and HD 164249. The MIPS detections for these latter targets could include background sources that cannot be distinguished from the target stars, but as we argue above, this is relatively unlikely, $<1\%$. It is more likely that some of the fixed parameters need to vary and that measurements are needed at other wavelengths to constrain the models. Both of these objects are also not particularly well fit by the simple blackbodies above. HD 164249 was called out as a particularly poor fit above; with the more sophisticated modeling (given the constrained parameters above), the 24 μm excess can be fit, but the 70 μm model is well below the observed flux. AG Tri A's simple blackbody fit above runs through the upper limit at 160 μm, and if the true flux of the system is really much lower, the simple fit will not work either.

4.5.4. *Testing the Simple Models by Including IRS Data*

Three stars have IRS spectra as noted above and as reported in Chen et al. (2006)—η Tel, HD 181327, and HR 7012. (Additional IRS spectra for several more BPMG stars exist in the *Spitzer* archive, but analyzing those data is beyond the scope of this paper.) As a simple way of assessing the limitations of the simple models

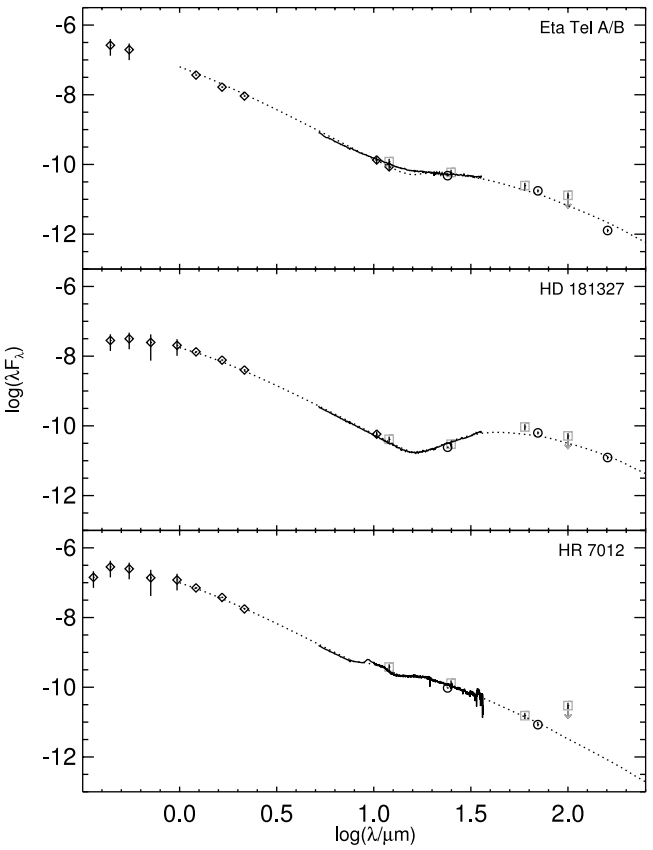

FIG. 9.—Same as Fig. 8, but for the three stars with IRS spectra considered for unconstrained modeling; see text for details of the modeling.

performed above that primarily rely on the MIPS data in the mid- and far-IR, for η Tel, HD 181327, and HR 7012, we included the IRS data and then attempted an unconstrained Mannings et al. model fit, e.g., letting all of the parameters vary. Plots of these fits (including the IRS data from Chen et al. 2006) appear in Figure 9.

For η Tel, the constrained model fit above slightly underpredicts the 70 μm flux density (by 17%) while slightly overpredicting the 160 μm flux density (by 10%). In order to fit the IRS data as well, the best model fit now brings the inner radius in from 70 to 30 AU, and the disk mass from 0.8 to 0.3 $M_{\rm moon}$.

For HD 181327, the constrained model fit above predicts a higher 24 μm flux than is observed. In order to allow the model to fit the IRS+MIPS data together, but still leave the inner disk radius constrained to that reported by Schneider et al. (2006), we increased the minimum grain size from 0.001 to 1 μm, so the grains are distributed as a power law from 1 μm to 1 mm. The model matches the IRS spectrum very well, eliminating the discrepancy at 24 μm, but slightly underpredicting (by 17%) the 70 μm flux while slightly overpredicting (by 10%) the 160 μm flux. The disk mass increases from the 9 $M_{\rm moon}$ reported above to 11 $M_{\rm moon}$.

Finally, for HR 7012, the best-fit disk mass is identical to the fit as reported above (0.05 $M_{\rm moon}$) and the inner disk radius changes from 5 to 3.5 AU, not a significant change. The model replicates well the emission features observed near 10 and 20 μm, so the grains in this disk could be silicate or have a large silicate component, as reported by Chen et al. (2006).

5. DISCUSSION

Based on the standard paradigm, the stars in the BPMG are expected to have a lower disk frequency and smaller infrared excesses than that found in younger stars, and to possess a higher

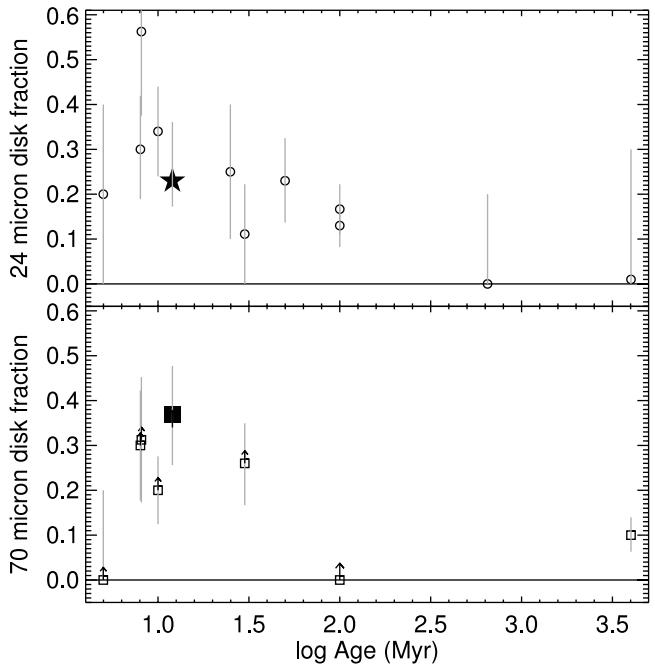

FIG. 10.—Evolution of disk fraction with time: the top panel is the 24 μm disk fraction, and the bottom panel is the 70 μm disk fraction. Values from the literature (see Table 5) are compared with our values for the BPMG. Literature 24 μm points are circles, the BPMG 24 μm point is a large solid five-pointed star, literature 70 μm points are boxes, and the BPMG 70 μm point is a large solid box. The gray vertical lines are the errors calculated from Poisson (counting) statistics. Our points are consistent with the disk fractions for similarly aged clusters and associations found in the literature.

disk frequency and larger excesses than older stars. Our results follow those expectations at both 24 and 70 μm; Figure 10 plots our 24 and 70 μm disk (excess) fractions in context with several other determinations from the literature, which can also be found in Table 5. After a brief discussion of some minor issues, we now discuss our study in the context of other studies in the literature.

Because these disks are likely to evolve such that the infrared excesses disappear from the "inside out" (e.g., Su et al. 2006) it is important to consider the wavelength dependence of the disk fraction being considered. Since the sensitivity of the 70 μm array does not allow for detections of the stellar photospheres for most stars, it is difficult to obtain an unambiguous definition of the disk fraction at this wavelength. Essentially all studies, therefore, quote a lower limit to the true 70 μm disk fraction in clusters or associations. The error bars shown in Figure 10 and listed in Table 5 are derived from Poisson (counting) statistics. Note too that there are relatively large uncertainties on the ages of these clusters and associations. Finally, we note that several of our stars as considered here are unresolved binaries. We have made no attempt to distinguish binaries as a separate population from single stars here, or to apportion the flux between the companions, but we have listed known binarity in Tables 1–3. Given the distance of the BPMG and the MIPS resolution, unresolved binaries must have a separation of $\lesssim$200 AU. The results of Trilling et al. (2007) suggest that the evolution of such circumbinary disks is roughly comparable to that of single stars, so including unresolved binaries as single stars should not significantly change Figure 10.

There are three associations in Table 5 thought to be younger than the BPMG: Upper Sco ($\sim$5 Myr), the TW Hydra association (TWA; $\sim$8–10 Myr), and the η Chamaeleon association ($\sim$5–9 Myr). All three of these associations have larger 24 μm disk fractions in the literature (Chen et al. 2005a; Low et al. 2005; Gautier et al. 2008, respectively) than we find for the BPMG, consistent with expectations. (Admittedly, the Upper Sco sample includes only about 5% of the likely members of this association, so there is a large uncertainty on the disk fraction compared to what future investigators are likely to conclude.) Low et al. (2005) find for TWA that there are very large excesses around four of the TWA stars, with possibly a subtle 24 μm excess around one more of the stars. We have rereduced their MIPS data in exactly the same fashion as here in the BPMG and find, as did Low et al., that many of the measurements are consistent with photospheres. We were able to measure 24 μm fluxes for 23 objects, some of which are components of wide binary systems. We confirm the 4 large excess objects (TWA 1, 3, 4, and 11), as well as the small excess found in TWA 7, but also, using the same criteria as for the BPMG, that 8b and 19 are also likely to harbor circumstellar disks. Thus, to aid in direct comparison with our BPMG data, we have taken the TWA disk fraction at 24 μm to be 7/23 stars, or 30%. The largest excess objects in TWA have $K_s - [24] > 4$ (5.8, 5.0, 4.4, and 4.4 for TWA 1, 3, 4, and 11, respectively, with $F_{\rm meas}/F_{\rm pred} = 160$, 69, 51, and 58). The reddest object we have is β Pic itself, with $K_s - [24]$ of only 3.5, well below the four extreme TWA stars. The three TWA stars with more moderate excesses, TWA 7, 8b, and 19, have $K_s - [24] = 0.70$, 0.75, and 0.30, respectively. (The $F_{\rm meas}/F_{\rm pred}$ values we calculate are 1.4, 1.3, and 1.3, respectively.) In terms of the 70 μm disk fraction, the

TABLE 5
INFRARED EXCESS FRACTIONS

Cluster/Association	Age (Myr)	24 μm Disk Fraction	70 μm Disk Fraction	Reference
Upper Sco F and G	$\sim$5	1/5, 20% ($\pm$20%)	0/5, >0% ($\pm$20%)	Chen et al. (2005a)
η Cha	$\sim$8	9/16, 56% ($\pm$18%)	5/15, >33% ($\pm$15%)	Gautier et al. (2008)
TW Hya	$\sim$8	7/23, 30%[a] ($\pm$11%)	6/20, >30% ($\pm$10%)	Low et al. (2005)
UCL and LCC[b] F and G	$\sim$10	12/35, 34% ($\pm$10%)	7/35, >20% ($\pm$7%)	Chen et al. (2005a)
BPMG	$\sim$12	7/30, 23% ($\pm$9%)	11/30, >37% ($\pm$11%)	This work
Tuc-Hor	$\sim$30	1/9, 11% ($\pm$11%)	8/31, >26% ($\pm$10%)	Smith et al. (2006), combined with this work
NGC 2547	$\sim$25	$\sim$25%	...	Young et al. (2004)
IC 2391	$\sim$50	6/26, 23% ($\pm$9%)	...	Siegler et al. (2007)
Pleiades	$\sim$100	9/54, 17% ($\pm$5%)	None detected	Gorlova et al. (2006), Stauffer et al. (2005)
M47	$\sim$100	8/63, 13% ($\pm$5%)	...	Gorlova et al. (2004)
Hyades	$\sim$650	0/6, 0% ($\pm$2%)	...	Rieke et al. (2005)
Field	$\sim$4000	1/69, 1% ($\pm$3%)	7/69, 10% ($\pm$4%)	Bryden et al. (2006)

[a] TWA 24 μm infrared excess fraction reassessed here; see text for discussion.
[b] UCL=Upper Centaurus-Lupus; LCC=Lower Centaurus-Crux.

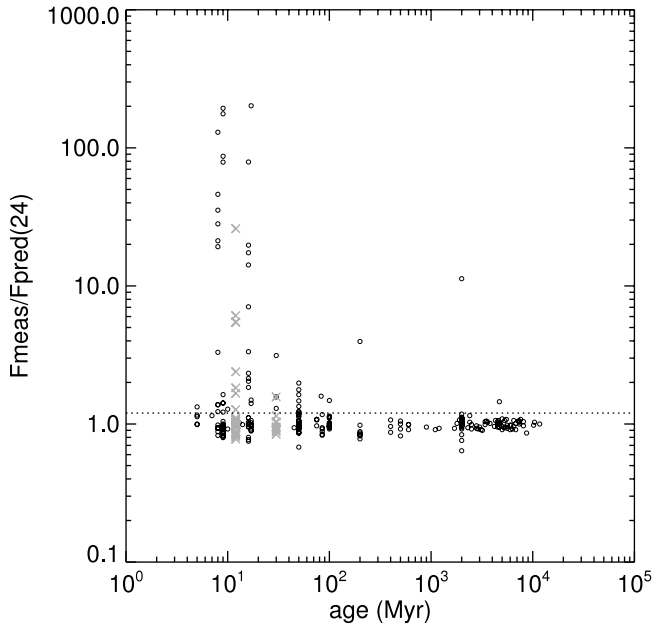

FIG. 11.—Ratio of measured to predicted 24 μm flux as a function of time for objects in the literature, as described in the text; gray times symbols correspond to our objects from the BPMG and Tuc-Hor. The horizontal dotted line corresponds to the $F_{\rm meas}/F_{\rm pred} = 1.2$ cutoff between disks and photospheres discussed in § 3.1.

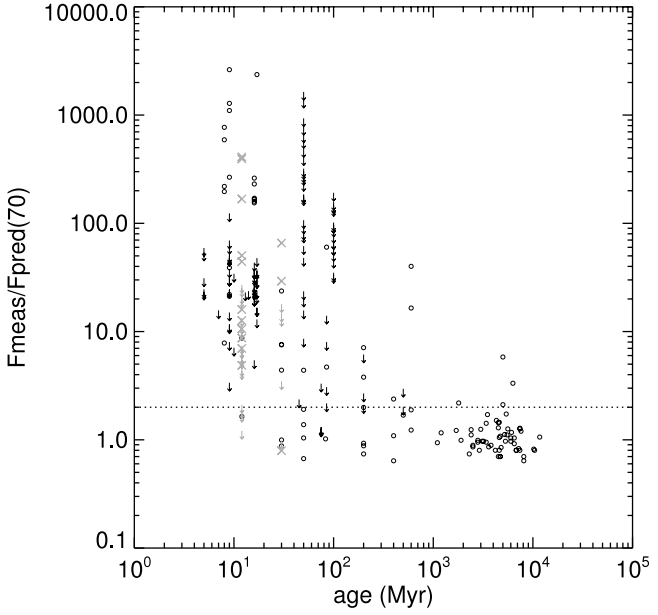

FIG. 12.—Ratio of measured to predicted 70 μm flux as a function of time for objects in the literature, as described in the text; gray times symbols or upper limits correspond to our objects from the BPMG and Tuc-Hor. The horizontal dotted line corresponds to the $F_{\rm meas}/F_{\rm pred} = 2$ cutoff between disks and photospheres discussed in § 3.2.

numbers obtained for Upper Sco, TWA, η Cha, and the BPMG are all consistent, within 1 σ uncertainties, with having a constant disk fraction. The one disk candidate from the Chen et al. (2005a) Upper Sco sample has $L_{\rm dust}/L_* = 4.4 \times 10^{-4}$. The values for $L_{\rm dust}/L_*$ for TWA range from 0.27 to $\sim 10^{-4}$ (Low et al. 2005), and in η Cha, they range from 0.019 to $\sim 10^{-6}$ (Gautier et al. 2008); both of these clusters have larger $L_{\rm dust}/L_*$ values than those we find here in the BPMG ($10-250 \times 10^{-5}$).

The estimated age of the Upper Centarus-Lupus (UCL) and Lower Centaurus-Crux (LCC) associations has been taken to be $\sim$15–20 Myr (e.g., Chen et al. 2005a), but more recently it has been set at $\sim$10 Myr (I. Song et al. 2008, in preparation), which we adopt here. The ages of those clusters are roughly comparable to that of the BPMG. Both the 24 and 70 μm disk fractions found in F and G stars from UCL and LCC are within 1 σ of the disk fractions found in the BPMG, despite the fact that our BPMG disk fractions include more stars than just F and G. The $L_{\rm dust}/L_*$ values found in UCL and LCC range from $\sim 10^{-3}$ to 10^{-5}, comparable to the range we find in the BPMG.

Tuc-Hor ($\sim$20–40 Myr) and NGC 2547 ($\sim$25 Myr) are thought to be slightly older than the BPMG. Membership in NGC 2547 (Young et al. 2004) is not as well established as it is for other objects in Table 5. The 24 μm disk fraction is consistent with that for the BPMG, and the 70 μm disk fraction is not reported. Working in a sample of nearby solar-type young stars (including several from but not limited to Tuc-Hor), Smith et al. (2006) find that just 19 of their overall 112-star sample (17%) have 70 μm detections at all. Of the 22 stars in the Tuc-Hor association included in the Smith et al. sample, 8 are detected and 6 are determined to be greater than photospheric, for a lower limit on the disk fraction of 27%. We can combine these stars with the 9 Tuc-Hor stars from the present work, obtaining a 24 μm disk fraction of 1/9 (11%), and a 70 μm disk fraction of at least 8/31 (>26%). Given small-number statistics, the Tuc-Hor disk fractions at both 24 and 70 μm are indistinguishable from those obtained here in the BPMG.

There are four clusters, in addition to field stars, older than the BPMG in Table 5. The 24 μm disk fraction reported by Siegler et al. (2007) for IC 2391 ($\sim$50 Myr) is comparable to that for the BPMG. The disk fractions from the Pleiades and M47 ($\sim$100 Myr; Gorlova et al. 2006, 2004) are only marginally lower than that inferred for the BPMG. The BPMG disk fraction is significantly higher than that for the Hyades (Rieke et al. 2005) or field stars from the solar neighborhood (Bryden et al. 2006). The Bryden et al. (2006) study found just one 24 μm excess out of 69 stars. Detections (of disks or photospheres) are harder at the distances of most of these older clusters; in the Pleiades, no disks are seen at 70 μm, although the background is quite high (Stauffer et al. 2005). For the old ($\sim$4000 Myr) field stars in Bryden et al. (2006), 10% of their $\sim$70 star sample has 70 μm disks. The $L_{\rm dust}/L_*$ values reported by Bryden et al. (2006) range from $<10^{-6}$ to $\sim 10^{-5}$, lower than what we find in the BPMG (or even could have detected). Our results are consistent with the trend that the disk fraction and brightness falls with time.

In considering these disk fractions, we have grouped together stars of a range of masses in order to increase the number of stars considered at each age; for example, the BPMG disk fraction includes stars from A to M. However, disk evolution is probably stellar-mass dependent (e.g., Carpenter et al. 2006), and certainly measured colors are mass dependent (as discussed above; see Fig. 6). Besides $L_{\rm dust}/L_*$, another way that we might attempt to compensate for the range of spectral types is to use the ratio of measured to predicted flux densities. Figures 11 and 12 present the ratios of predicted to measured flux densities for 24 and 70 μm for our stars and, where possible, values from the literature for individual stars (Bryden et al. 2006; Chen et al. 2005a, 2005b; Gautier et al. 2008; Kim et al. 2005; Low et al. 2005; Siegler et al. 2007; Smith et al. 2006; Stauffer et al. 2005). Where previous work has not reported a predicted flux density for each star, we have calculated the predicted flux densities by the same methodology as above for each star (finding the nearest grid point in the Kurucz-Lejeune model grid for a given spectral type and interpolating to the MIPS effective wavelengths). The upper envelope

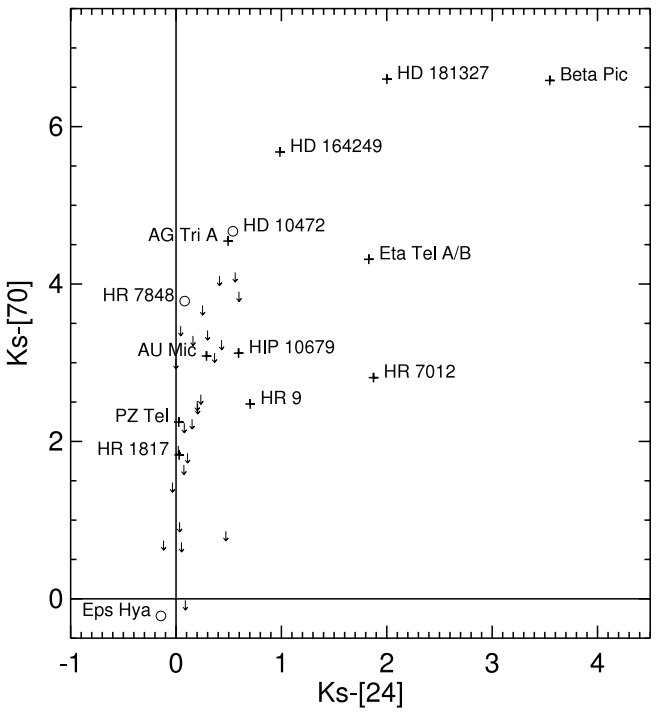

FIG. 13.—Plot of $K_s - [24]$ vs. $K_s - [70]$ for all of the objects considered here. Plus signs are objects detected (at 70 μm) from the BPMG; open circles are detected objects from Tuc-Hor. All other objects (from both associations) are indicated as upper limits at 70 μm. These results are consistent with an "inside-out" infrared excess reduction scenario, where 24 μm excesses disappear before 70 μm excesses; see text for further discussion.

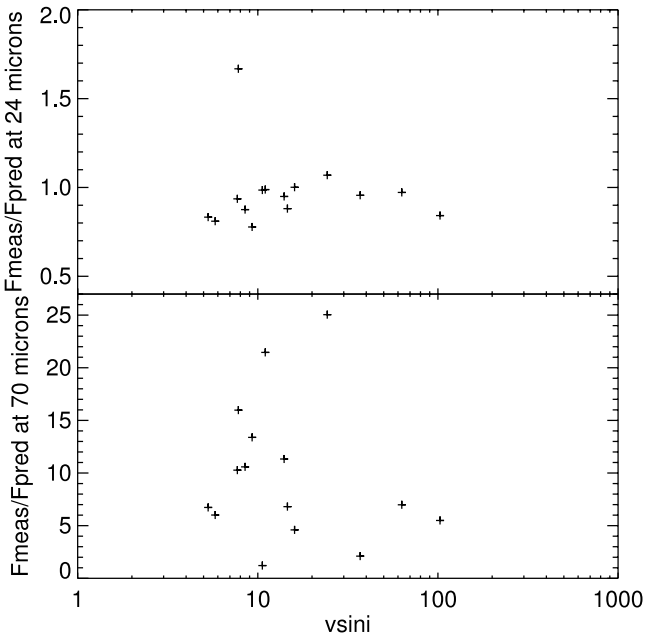

FIG. 14.—Plot of $v \sin i$ (in km s^{-1}) vs. $F_{\rm meas}/F_{\rm pred}$ at 24 μm (*top*) and at 70 μm (*bottom*) for all of the BPMG G, K, and M stars considered here. While certainly not conclusive, these figures are reminiscent of effects seen in younger clusters such as Orion.

found in these figures is similar to the 24 μm upper envelope found by Rieke et al. (2005) or Su et al. (2006) for 24 μm excesses around A stars, or at 70 μm by Su et al. (2006). The range of excess strengths found at any age could be a result of initial conditions, rates of evolution, or recent collisional events; there is no obvious way to determine the origin from these data alone. Currie et al. (2008) report seeing the decline of primordial disks and the rise of debris disks; this reinforces the importance of further study of stars with a range of excesses in the 8–10 Myr age range, specifically the need for high-quality complete disk fractions.

Figure 13 shows $K_s - [24]$ vs. $K_s - [70]$ for the objects considered here. It is clear not only which stars with excesses in one band also have excesses in the other band, but also very roughly the correlation of the size of the excess (with all the caveats about spectral type dependence discussed above). The MIPS measurements of ϵ Hya are consistent with a purely photospheric origin for its IR flux. Of the eight stars identified above as having any excesses at 24 μm, all also have clear excesses at 70 μm. All four objects with the largest 24 μm excesses also have large 70 μm excesses. Five additional stars are detected as having excesses at 70 μm, but without significant excesses at 24 μm. For the stars with disk excesses at 24 μm, the median $K_s - [24]$ is 0.99 mag; for those same stars, the median $K_s - [70]$ is 4.5 mag, significantly redder.

A disk may be inferred to have an inner hole if it has an infrared excess at long wavelengths but not at short wavelengths, such as these stars with significant 70 μm excess and very small 24 μm excess. By this definition, the majority of debris disks around older main-sequence FGK stars possess inner holes (29 of 37 disks; Trilling et al. 2008), whereas only 8/44 debris disks around younger A stars do (Su et al. 2006). At ages of a few megayears, the circumstellar disks found in star-forming regions have a very low MIPS inner hole frequency (Rebull et al. 2007; Harvey et al. 2007; Young et al. 2005). MIPS studies of young associations such as the BPMG provide a key bridge between the massive, young disks that generally lack inner holes and the older, tenuous debris disks that often possess them. At age 8 Myr, the TW Hya and η Cha groups show very few disks with MIPS inner holes (1/6 disks from TWA, Low et al. 2005 and reduction above; and 0/5 disks from η Cha, Gautier et al. 2008). These young associations also possess a mixed population of disks with fractional infrared luminosities near 0.1 (characteristic of massive primordial disks, such as that of TW Hya) and <0.001 (characteristic of optically thin debris disks, such as that of β Pic). None of the stars with disks in the larger Sco-Cen association (part of which is age $\sim$5 Myr and the rest of which is age $\sim$10 Myr) possess MIPS inner holes (Chen et al. 2005a). The 12 Myr old BPMG (this work) contains only optically thin disks, with 4/11 disks possessing MIPS inner holes (note that we are including AG Tri A, since it has a proportionally much larger 70 μm excess than any potential small 24 μm excess). In the $\sim$30 Myr old Tuc-Hor association, 6/8 stars with disks have inner holes (this work, combined with Smith et al. 2006). A smooth increase of inner hole frequency with time is evident, and although small number statistics prevent strong conclusions, it is clear that the BPMG is the youngest stellar group in which the frequency of MIPS inner holes is clearly larger than that seen in the pre-main-sequence stellar population. What is seen in the BPMG and these other clusters is consistent with expectations based on other clusters that stars lose their 24 μm excesses before their 70 μm excesses ("inside-out"; e.g., Su et al. 2006).

The G, K, and M stars in at least some clusters that are much younger than the BPMG, $\sim$1–5 Myr old, exhibit a correlation between rotation and infrared excess in that slower rotators are more likely to have infrared excesses, or disks (see, e.g., Rebull et al. 2006 and references therein). This agrees with theoretical expectations in that the young lower mass GKM stars are thought to have strong magnetic fields that thread the (primordial) circumstellar disk, mediating accretion and locking the rotation of the star to that of the disk. However, by the $\sim$12 Myr age of the

TABLE 6
$v \sin i$ Values Used for BPMG Stars G0 and Later

Star	$v \sin i$ (km s^{-1})
HIP 10679	7.8
HIP 12545	9.3
GJ 3305	5.3
HIP 23309	5.8
GJ 3322 A/B	7.7
AO Men	16
V343 Nor A/B	11
V824 Ara A/B	37 (companion 34)
CD −64 1208 A/B	102.7
PZ Tel	63
AT Mic A/B	10.6 (companion 17)
AU Mic	8.5
AZ Cap A/B	14.6
WW PsA A	14.0
WW PsA B	24.3

BPMG, and at the distances from the parent star of these disks emitting at 24 and 70 μm, it is not expected that disk locking will still be operating. In Figure 14, we examine the correlation of disk excess with rotation rates for the G, K, and M BPMG members. (The $v \sin i$ values used for these stars appear in Table 6.) The faster rotating lower mass stars in the BPMG in Figure 14 show a *weak* tendency to have a smaller disk excess. While certainly not conclusive, these figures are suggestive. Additional $v \sin i$ and rotation period determinations would be useful to test this correlation, as well as additional *Spitzer* measurements in other similarly aged clusters. Interestingly, Stauffer et al. (2007) find a similar correlation between 24 μm excess and $v \sin i$ seen in open clusters primarily from the FEPS program (Formation and Evolution of Planetary Systems; Meyer et al. 2006) and the Pleiades. Given that all of our disk candidates in the BPMG now possess at best tenuous debris disks, the disk mass is insufficient (now) to regulate the stellar angular momentum as in the case of massive primordial disks. Perhaps these disks started out as more massive than the other BPMG members. Perhaps the disk dispersion timescale, which determines whether or not a disk still persists at $\sim$12 Myr, is set early on in the lifetime of the disk, when the angular momentum and mass flux through the disk is the highest, the central object is large, and the influence of disk locking (or braking) is the strongest. In that case, the *weak* correlation seen in Figure 14 is the signature of a process operating at earlier times.

Alternatively, strong stellar winds could play an important role in clearing the disk of small particles, as suggested by Plavchan et al. (2005) and Chen et al. (2005a). Rapid rotation, which enhances the stellar dynamo and presumably the strength of the stellar wind, would then be associated with more tenuous disks as suggested by the data in Figure 14. Wind ablation of dust could be an ongoing process.

We see no obvious way to test for whether winds (operating now and/or in the past) or disk locking (operating in the past) are more likely using these data; clearly these initial results will need future observational follow-up, such as the use of periods rather than $v \sin i$ and a search for similar effects in other similarly aged clusters. We emphasize again for clarity that the correlation seen in Figure 14 is only for the GKM stars in the BPMG.

6. CONCLUSIONS

We have presented here MIPS 24 and 70 μm observations of 30 stars or star systems in the BPMG, as well as 9 from Tucana-Horologium, with 160 μm observations for a subset of 12 BPMG stars. In several cases, the new MIPS measurements resolve source confusion and background contamination issues in the previous *IRAS* data.

We found that 7 BPMG members have significant 24 μm excesses, or a disk fraction of 23%. Eleven BPMG systems have significant 70 μm excesses (disk fraction of $\geq$37%, as this is a lower limit). Five exhibit 160 μm excesses, out of a biased sample of 12 observed, and they have a range of 70 : 160 μm flux ratios. The disk fraction and the size of the excesses measured at each wavelength are both consistent with an "inside-out" infrared excess reduction scenario, wherein the shorter wavelength excesses disappear before longer wavelength excesses, and consistent with the overall decrease of disk frequency with stellar age, as seen in *Spitzer* studies of other young stellar groups.

We characterized the disk properties using simple models and fractional infrared luminosities. Optically thick disks, seen in the 8 Myr age TW Hya and η Cha associations, are entirely absent in the BPMG at age 12 Myr.

L. M. R. wishes to acknowledge funding from the *Spitzer* Science Center to allow her to take a "science retreat" to work intensively on this paper. The authors wish to acknowledge the MIPS GTO team for allowing us to use the DAT to process the 160 μm data. This work is based on observations made with the *Spitzer Space Telescope*, which is operated by the Jet Propulsion Laboratory, California Institute of Technology, under a contract with NASA. Support for this work was provided by NASA through an award issued by JPL, Caltech. This research makes use of data archived and served by the NASA Star and Exoplanet Database (NStED) at the Infrared Processing and Analysis Center. NStED is jointly funded by the National Aeronautics and Space Administration (NASA) via Research Opportunities in Space Sciences grant 2003 TPF-FS, and by NASA's Michelson Science Center. NStED is developed in collaboration with the NASA/IPAC Infrared Science Archive (IRSA). This research has also made use of NASA's Astrophysics Data System (ADS) Abstract Service, and of the SIMBAD database, operated at CDS, Strasbourg, France. This research has also made use of data products from the Two Micron All-Sky Survey (2MASS), which is a joint project of the University of Massachusetts and the Infrared Processing and Analysis Center, funded by NASA and the National Science Foundation. These data were served by the NASA/IPAC Infrared Science Archive, which is operated by JPL, Caltech, under contract with NASA. The research described in this paper was partially carried out at JPL, Caltech, under contract with NASA.

APPENDIX A

COMMENTS ON INDIVIDUAL OBJECTS

These comments on individual objects address the issues of (possibly) resolved objects, serendipitous detections, IR cirrus, and multiple systems. In some cases, the proximity of a true companion and/or infrared cirrus results in the low spatial resolution *IRAS* fluxes being anomalously high when compared with the MIPS fluxes. All of those instances are discussed here.

In several cases, objects in close proximity to the target object were detected. Since these objects are bright enough to be detected in these shallow observations, these additional objects are also potential association members, and/or contributors to source confusion in lower spatial resolution observations such as *IRAS*. Based on the MIPS measurements, we conclude that none are association members; see individual discussion below.

A1. HIP 3556 (TUC-HOR)

At 24 μm, there are several objects easily visible besides the target, with several being of comparable brightness to the target. Two of them are easily visible in the 70 μm image, whereas HIP 3556 is undetected. Few of them have obvious counterparts in a POSS or 2MASS image. Given their evidently steeply rising SEDs, we suspect that they are background galaxies.

A2. ϕ ERI (TUC-HOR)

Spitzer observations of ϕ Eri clearly detect it in 24 μm to be 173 mJy; there is an emission peak at this location at 70 μm, but it is comparable in size to the noise fluctuations found in this region, so it is listed as an upper limit in our study. The upper limit falls right on the expected photospheric flux.

There is a nearby source 90″ away at $02^{h}16^{m}30.6^{s}$, $-51^{\circ}30^{m}44^{s}$, measured to be 12.3 mJy (at 24 μm). This object is not detected at 70 μm, but it is detected in 2MASS with $K_s = 4.13$ mag. The resultant $K_s - [24]$ color suggests that it is far too blue to be a star, but the PSF as seen in POSS plates appears stellar. This source is probably not a new association member.

A3. HD 14082 and HIP 10679

HIP 10679 and HD 14082 are close enough to each other ($\sim$10″) to be observed in the same MIPS photometry field of view. Both objects are point sources at 24 μm and have comparable fluxes at this bandpass. At this separation, these objects should be distinguishable at 70 μm, but only one object is detected. Based on the central position of the object, we have assigned the measured flux to HIP 10679. This is a weak detection, with a S/N of only $\sim$5. The PSF appears to be elliptical, with the major axis larger than the minor axis by roughly a factor of 2. It is not extended in the direction of the companion or in the direction of the scan mirror motion. While it is possible that the object is truly resolved at 70 μm, the fact that it is not resolved at 24 μm leads us to suspect that the apparently elliptical PSF is instrumental in nature. The object is so faint as to not be easily detectable in subsets of the data, so it is difficult to assess whether or not co-adding the data has caused this effect.

A4. GSC 8056-482 (TUC-HOR)

While only one BPMG object is expected to be included in this observation, several fainter objects are clearly detected in the 24 μm image. The brightest one, which is also closest to GSC 8056-482, is 23″ away, located at $02^{h}36^{m}49.1^{s}$, $-52^{\circ}03^{m}12.3^{s}$, and is measured to be 2.0 mJy. It is not detected in 2MASS or at 70 μm.

A5. HR 6070

HR 6070 appears in the *IRAS* PSC (but not the FSC) as a detection at all *IRAS* bands, with coordinates slightly offset to the northwest from the optical position. However, the MIPS observations reveal an isolated point source with lower flux measured at 24 μm and an upper limit at 70 μm that is comparable to the detection reported by *IRAS*. The 24 μm image reveals clear cirrus on the northwest side of the image, in the same direction as the reported center of the *IRAS* source, suggesting that the measured *IRAS* flux is contaminated by infrared cirrus. If all of the flux attributed to the point source in the *IRAS* catalog were really coming from the point source, we would have detected it, but we did not. The MIPS observations provide a much better understanding of any infrared excess present in this star, suggesting no excess at 24 μm and providing a constraint at 70 μm.

A6. V824 ARA A, B, AND C

This triple system, located all within an arcminute, was also unresolved by *IRAS*. MIPS can clearly separate C from A/B at 24 μm, but no objects are detected at 70 μm. *IRAS*'s beam size encompasses all three of these components. MIPS resolves the source confusion and does not find an IR excess in A/B or C.

In addition to the components of this system, MIPS sees two additional objects, neither of which are seen at 70 μm. Neither of these objects have a $K_s - [24]$ color suggestive of an excess.

A7. HD 164249

In the 24 μm image for HD 164249, three objects are present, two of which are also seen at 70 μm. (None of the objects is seen in our 160 μm data.) The target of the observation is clearly apparent in both 24 and 70 μm, and a second object appears 0.76′ away, with a 24 μm flux of 1220 mJy and a 70 μm flux of 172 mJy. A third faint object 1.4′ away has a 756 μJy flux at 24 μm. Both of these objects appear in the 2MASS catalog. The brighter object has a $K_s - [24]$ color of 7.4; the fainter object has $K_s - [24] = 0.002$. The latter is a photosphere with arguably no excess whatsoever at 24 μm. This, combined with its overall faintness, suggests that it is probably a background star. The former appears as a very faint smudge on POSS plates and has a clear elliptical shape in 2MASS images. The

object appears in the 2MASS extended source catalog as a galaxy with name 2MASX J18030752−5139225. It likely has influenced the measured flux for HD 164249 in lower spatial resolution measurements.

A8. HR 6749/HR 6750

This binary system is unresolved by MIPS. *IRAS* measures a detection at all four bands, suggesting an infrared excess and therefore circumstellar dust. MIPS is able to resolve apparent source confusion, placing the 24 μm point at a photospheric level and putting constraints on the 70 μm flux. The 24 μm image suggests that there may be infrared cirrus that contributed to the measured *IRAS* flux; any background flux is not very bright at MIPS-24 (while MIPS has much more sensitive detectors that *IRAS*, it also samples much smaller angles on the sky, so the surface brightness sensitivity is not substantially different than *IRAS*). At 70 μm, if all of the flux attributed to the point source in the *IRAS* catalog were really coming from the point source, we would have detected it, but we did not.

A9. AT MIC

This object is detected at 24 μm, but not at 70 μm. There is another object at 24 μm that is 1.5′ away, at $20^{h}41^{m}55.4^{s}$, $-32^{\circ}24^{m}57^{s}$, with a 24 μm flux of 2.8 mJy. This object has a $K_s - [24]$ color of −0.02, which is not indicative of any excess.

A10. RESOLVED OBJECTS

We note for completeness that at least three objects in the BPMG, β Pic itself (e.g., Golimowski et al. 2006), AU Mic (e.g., Graham et al. 2007), and HD 181327 (e.g., Schneider et al. 2006), are known to be resolved at other wavelengths. AG Tri A may be resolved as well (D. Ardila et al. 2008, in preparation). Of these, β Pic itself is the only one known to be resolved at MIPS wavelengths (K. Su et al. 2008, in preparation; see also Chen et al. 2007); the others, if they are resolved at MIPS wavelengths, are only subtly larger than the instrumental PSF. All of these famous objects are extensively discussed elsewhere, so we do not discuss them again here.

REFERENCES

Ali, B., et al. 2005, BAAS, 37, 1409
Barrado y Navascues, D., et al. 1999, ApJ, 520, L123
Beichman, C. A., et al. 1988, IRAS Catalogs and Atlases, Volume 1 (Pasadena: Caltech)
Bohren, C. F., & Huffman, D. R. 1983, Absorption and Scattering of Light by Small Particles (New York: Wiley)
Bryden, G., et al. 2006, ApJ, 636, 1098
Carpenter, J., et al. 2006, ApJ, 651, L49
Chen, C., & Jura, M. 2001, ApJ, 560, L171
Chen, C., et al. 2005a, ApJ, 623, 493
———. 2005b, ApJ, 634, 1372
———. 2006, ApJS, 166, 351
———. 2007, ApJ, 666, 466
Currie, T., et al. 2008, ApJ, 672, 558
Dole, H., et al. 2004, ApJS, 154, 87
Engelbracht, C., et al. 2007, PASP, 119, 994
Feigelson, E., et al. 2006, AJ, 131, 1730
Gautier, N., et al. 2007, ApJ, 667, 527
———. 2008, ApJ, in press
Gillett, F. 1986, in Light on Dark Matter, ed. F. P. Israel (Dordrecht: Reidel), 61
Golimowski, D., et al. 2006, AJ, 131, 3109
Gordon, K., et al. 2005, PASP, 117, 503
———. 2007, PASP, 119, 1019
Gorlova, N., et al. 2004, ApJS, 154, 448
———. 2006, ApJ, 649, 1028
Graham, J., et al. 2007, ApJ, 654, 595
Harvey, P., et al. 2007, ApJ, 663, 1139
Houck, J., et al. 2004, ApJS, 154, 18
Houk, N., et al. 1982, Michigan Spectral Survey, Volume 3 (Ann Arbor: Univ. Michigan)
Jayawardhana, R., et al. 2006, ApJ, 648, 1206
Kaisler, D., et al. 2004, A&A, 414, 175
Kalas, P., et al. 2004, Science, 303, 1990
Kenyon, S. J., & Bromley, B. C. 2002, ApJ, 577, L35
Kim et al. 2005, ApJ, 632, 659
Krist, J. 2005, Tiny Tim for Spitzer (Pasadena: Caltech), http://ssc.spitzer.caltech.edu/archanaly/contributed/stinytim/index.html
Krist, J. E., et al. 2005, AJ, 129, 1008
Lejeune, T., Cuisinier, F., & Buser, R. 1997, A&AS, 125, 229
———. 1998, A&AS, 130, 65
Low, F., Smith, P. S., Werner, M., Chen, C., Krause, V., Jura, M., & Hines, D. 2005, ApJ, 631, 1170
Makovoz, D., & Marleau, F. 2005, PASP, 117, 1113
Mamajek, E., et al. 2004, ApJ, 612, 496
Mathis, J. S., Rumpl, W., & Nordseick, K. H. 1977, ApJ, 217, 425
Meyer, M., et al. 2006, PASP, 118, 1690
———. 2007, in Protostars and Planets V, ed. B. Reipurth, D. Jewitt, & K. Keil (Tucson: Univ. Arizona Press), 573
Moshir, M., Kopman, G., Conrow, T. 1992, IRAS Faint Source Survey and Explanatory Supplement (Pasadena: Caltech)
Paresce, F., & Burrows, C. 1987, ApJ, 319, L23
Plavchan, P., Jura, M., & Lipscy, S. J. 2005, ApJ, 631, 1161
Rebull, L., et al. 2006, ApJ, 646, 297
———. 2007, ApJS, 171, 447
Rieke, G., et al. 2004, ApJS, 154, 25
———. 2005, ApJ, 620, 1010
Schneider, G., et al. 2006, ApJ, 650, 414
Siegler, N., et al. 2007, ApJ, 654, 580
Skrutskie, M., et al. 2006, AJ, 131, 1163
Smith, P. S., Hines, D., Low, F., Gehrz, R., Polomski, E., & Woodward, C. 2006, ApJ, 644, L125
Song, I., et al. 2003, ApJ, 599, 342
Stansberry, J., et al. 2007, PASP, 119, 1038
Stauffer, J., et al. 2005, AJ, 130, 1834
———. 2007, in Poster Proc. IAU Symp. 243, Star-Disk Interaction in Young Stars, ed. J. Bouvier & I. Appenzeller (Cambridge: Cambridge Univ. Press), http://www.iaus243.org/IMG/pdf/stauffer.pdf
Su, K., et al. 2004, BAAS, 36, 1366
———. 2006, ApJ, 653, 675
Sylvester, R. J., & Skinner, C. J. 1996, MNRAS, 283, 457
Torres, C., et al. 2006, A&A, 460, 695
Trilling, D., et al. 2007, ApJ, 658, 1289
———. 2008, ApJ, 674, 1086
Werner, M., et al. 2004, ApJS, 154, 1
———. 2006, ARA&A, 44, 269
Young, E., et al. 2004, ApJS, 154, 428
Young, K., et al. 2005, ApJ, 628, 283
Zuckerman, B., & Song, I. 2004, ARA&A, 42, 685
Zuckerman, B., Song, I., & Webb, R. 2001a, ApJ, 559, 388
Zuckerman, B., et al. 2001b, ApJ, 562, L87